The influence of water-saturation on the strength of volcanic rocks and the stability of lava domes

Michael J Heap, Claire Harnett, Jamie Farquharson, Patrick Baud, Marina Rosas-Carbajal, Jean-Christophe Komorowski, Marie E.S. Violay, H. Albert Gilg, Thierry Reuschlé

The influence of water-saturation on the strength of volcanic rocks and the stability of lava domes

Michael J. Heap[1,2]*, Claire Harnett[3]*, Jamie Farquharson[4,5], Patrick Baud[1], Marina Rosas-Carbajal[6], Jean-Christophe Komorowski[6], Marie E.S. Violay[7], H. Albert Gilg[8], and Thierry Reuschlé[1]

[1] *Université de Strasbourg, CNRS, Institut Terre et Environnement de Strasbourg, UMR 7063, 5 rue René Descartes, Strasbourg F-67084, France*

[2] *Institut Universitaire de France (IUF), Paris, France*

[3] *School of Earth Sciences, University College Dublin, Dublin, Ireland*

[4] *Institute for Research Administration, Niigata University, Ikarashi 2-8050, Nishi-ku, Niigata 950-2181, Japan*

[5] *Research Institute for Natural Hazards and Disaster Recovery, Niigata University, Ikarashi 2-8050, Nishi-ku, Niigata 950-2181, Japan*

[6] *Université de Paris Cité, Institut de Physique du Globe de Paris, CNRS, F-75005 Paris, France*

[7] *Laboratory of Experimental Rock Mechanics, Ecole Polytechnique Fédérale de Lausanne, Lausanne, Switzerland*

[8] *TUM School of Engineering and Design, Technical University of Munich, Arcisstrasse 21, 80333 Munich, Germany*

*Corresponding authors: Michael Heap (heap@unistra.fr) and Claire Harnett (claire.harnett@ucd.ie)

Abstract

The rocks forming a volcanic edifice or dome are typically saturated or partially-saturated with water. However, most experiments aimed at better understanding the mechanical behaviour of volcanic rocks have been performed on dry samples, and therefore most large-scale models designed to explore volcano stability have used parameters representative for dry rock. Here, we present a combined laboratory and modelling study in which we (1) quantified the influence of water-saturation on the mechanical behaviour of variably altered dome rocks from La Soufrière de Guadeloupe (Eastern Caribbean) and (2) used these new data to investigate the influence of water on dome stability. Our laboratory data show that the ratio of wet to dry uniaxial compressive strength (UCS) and Young's modulus are ~0.30–0.95 and ~0.10–1.00, respectively. In other words, the dome rocks were all mechanically weaker when water-saturated. Further, the ratio of wet to dry UCS decreased with increasing alteration (the wt% of secondary minerals in the rocks). Micromechanical modelling suggests that the observed water-weakening is the result of a decrease in fracture toughness (K_{IC}) in the presence of water. The ratio of wet to dry K_{IC} also decreases with increasing alteration, explaining why water-weakening increased as a function of alteration. To explore the influence of water-saturation on lava dome stability, we numerically generated lava domes in Particle Flow Code using the experimental data corresponding to unaltered and altered rock under dry conditions. The strength of the dome-forming rocks was then reduced to values corresponding to wet conditions. Our modelling shows that, although the stability of the unaltered dome was not influenced by water-saturation, larger displacements were observed for the wet altered dome. Additional simulations in which we modelled a buried alteration zone within an otherwise unaltered dome showed that higher displacements were observed when the dome was water-saturated. We conclude that (1) the water-saturation reduces the UCS and Young's modulus of volcanic rock, (2) larger decreases in UCS in the

presence of water are observed for altered rocks, and (3) the stability of a dome can be compromised by the presence of water if the dome is altered, or contains an altered zone. These conclusions highlight that the degree of alteration and water-saturation should be mapped and monitored at active volcanoes worldwide, and that large-scale models should use values for water-saturated rocks when appropriate.

Highlights

- Water-saturation reduces the strength of volcanic rocks.
- Strength reduction in the presence of water is higher for altered volcanic rocks.
- Strength reduction in the presence of water can be explained by a reduction in fracture toughness.
- The stability of altered flanks and domes, or those containing altered zones, is jeopardised by water-saturation.

Keywords: hydrothermal alteration; uniaxial compressive strength; Young's modulus; fracture toughness; dome collapse

1 Introduction

The short- and long-term strength of rock is influenced not only by pore fluid pressures, but also by the presence of water within the void space (e.g., Baud et al., 2000; Brantut et al., 2013). Based on experiments and micromechanical analyses, reductions to the strength of rock associated with the presence of water are thought to be the result of a decrease in specific surface energy, friction coefficient, and fracture toughness (e.g., Baud et al., 2000; Noël et al., 2021), the presence of clay minerals (e.g., Hawkins and McConnell, 1992; Heap et al., 2019), adsorption pressures (e.g., Risnes et al., 2005), and/or an increase in the efficiency of sub-critical crack growth (e.g., Atkinson, 1984; Kranz et al., 1982; Masuda, 2001; Brantut et al., 2013; Tang et al., 2018).

Although water-weakening (the ratio of wet to dry strength) is reasonably well-documented for sedimentary rocks such as sandstone (e.g., Rutter and Mainprice, 1978; Chest and Logan, 1986; Hawkins and McConnell, 1992; Baud et al., 2000; Duda and Renner, 2013; Wasantha and Ranjith, 2014; Baud et al., 2015; Heap et al., 2019; Noël et al., 2021), carbonate rocks (e.g., Risnes et al., 2005; Baud et al., 2016; Nicolas et al., 2016; Castagna et al., 2018), and gypsum (e.g., Caselle et al., 2022), few data exist for volcanic rocks. For example, the onset of inelastic compaction in tuff from Alban Hills (Italy) was reduced by the presence of water (Zhu et al., 2011). The uniaxial compressive strength of tuffs containing alunite (Heap et al., 2015) and zeolites and clay minerals (Heap et al., 2018) was also lower in the presence of water. Zhu et al. (2016) found that the compressive strength of a basalt from Mt Etna (Italy) was reduced in the presence of water. Finally, the uniaxial compressive strength and Young's modulus of lava from Mount Unzen (Japan) (Kendrick et al., 2021) and the uniaxial compressive strength of lavas from Mt. Etna, Volvic (France), Kumamoto (Japan), and Volcán de Colima (Mexico) and a block-and-ash flow from Mt. Meager (Canada) (Heap and Violay, 2021) were reduced when saturated with water. While wet to dry

93 strength ratios in these lavas, which were relatively unaltered, were typically on the order of
94 ~0.9, this ratio in tuffs can reach ~0.2 when the tuffs are characterised by high zeolite and clay
95 mineral contents (Heap and Violay, 2021).

96 The importance of understanding the influence of water on the strength and
97 mechanical behaviour of volcanic rocks is threefold. First, volcanoes are often saturated or
98 partially-saturated and, in the case of subaerial, ocean-island, and coastal volcanoes, their
99 saturation state also varies as a function of space and time (Hurwitz et al., 2003; Join et al.,
100 2005; Aizawa et al., 2009; Delcamp et al., 2016). Volcanoes can be saturated, or partially-
101 saturated, with meteoric water (approximately 45% of the world's active volcanoes lie in the
102 Tropics and are therefore prone to intense periods of precipitation; Matthews et al., 2002),
103 magmatic fluids, and, in the case of submarine, ocean-island, and coastal volcanoes, seawater.
104 Second, modelling has shown that the mechanical properties of dome- and edifice-forming
105 rock plays a first-order role in dictating their stability and therefore the risk of collapse and
106 associated hazards (Apuani et al., 2005; Reid et al., 2001; Moon et al., 2009; Borselli et al.,
107 2011; Schaefer et al., 2013; Heap et al., 2021a, b; Harnett and Heap, 2021; Wallace et al.,
108 2022; Mordensky et al., 2022; Harnett et al., 2022; Carr et al., 2022; Heap et al., 2023a) and
109 so, if water-saturation reduces rock strength, it must also decrease dome and edifice stability.
110 As a result, volcano stability models should, where and when appropriate, use the mechanical
111 properties for water-saturated volcanic rocks. Third, the frequency of landslides and the
112 failure and collapse of volcanic slopes and domes increases following heavy rainfall (Kerle
113 and van Wyk de Vries, 2001; Matthews et al., 2002; Matthews and Barclay, 2004; Elsworth et
114 al., 2004; Simmons et al., 2004; Taron et al., 2007; Saucedo et al., 2008; Hicks et al., 2010;
115 Vázquez et al., 2022), which will likely be exacerbated by the increase in heavy rainfall
116 expected given the current trend in global warming (Farquharson and Amelung, 2022).

The paucity of laboratory data aimed at understanding water-weakening in volcanic rocks therefore hinders our ability to accurately assess the stability of volcanic domes and flanks. Further, not only does hydrothermal alteration, a very common process at active volcanoes worldwide, influence the physical and mechanical properties of volcanic rocks (e.g., Frolova et al., 2014; Pola et al., 2014; Wyering et al., 2014; Mordensky et al., 2018; Coats et al., 2018; Heap et al., 2021a, 2021b; Darmawan et al., 2022; Kanakiya et al., 2021, 2022; Schaefer et al., 2023), but altered rocks can also contain the minerals (e.g., alunite and clay minerals) that are thought to promote water-weakening in volcanic rocks, and so it is of particular importance to assess the influence of hydrothermal alteration on water-weakening in volcanic rocks. Indeed, a deadly debris avalanche at Casita volcano (Nicaragua) in 1998 was thought to be the combined result of hydrothermal alteration and heavy rainfall (van Wyk de Vries et al., 2000; Kerle and van Wyk de Vries, 2001; Kerle et al., 2003; Opfergelt et al., 2006), and a landslide on the northeastern side of the dome at Soufrière de Guadeloupe (Eastern Caribbean) that followed extreme rainfall exposed a collapse scar characterised by intensely hydrothermally altered materials (Figure 1b).

Here, therefore, we present the results of (1) experiments designed to assess the influence of water-saturation on the mechanical properties of variably-altered volcanic rocks and (2) large-scale numerical modelling in Particle Flow Code (PFC), informed by the experimental data, that investigates the influence of water on the stability of a volcanic dome. For the purpose of this study, we will use La Soufrière de Guadeloupe as a case study.

2 Case Study: La Soufrière de Guadeloupe (Eastern Caribbean)

La Soufrière de Guadeloupe is an active andesitic stratovolcano located on the French island of Guadeloupe in the Eastern Caribbean (Komorowski et al., 2005; Moretti et al., 2020; Figure 1a). Volcanic unrest at La Soufrière de Guadeloupe has been steadily increasing in the

last three decades, manifest as an increase in the number of acid chloride-sulfate springs and steam-dominated fumaroles, an increase in the heat output from the dome, an expansion of the outgassing area at the top of the dome, an increase in flank and summit displacement rates, and an abundance of shallow seismicity (including the largest felt tectonic earthquake since the last eruption in 1976–1977, and frequent earthquake swarms that include several hundreds of microearthquakes generated in few days and located within 1 km below the surface) (Brombach et al., 2000; Villemant et al., 2005; Tamburello et al., 2019; Moretti et al., 2020; Heap et al., 2021a; Jessop et al., 2021; Moune et al., 2022). Historically, partial edifice collapse has been common at La Soufrière de Guadeloupe: at least nine flank collapses have occurred in the last 9150 years (Boudon et al., 2008; Komorowski et al., 2005; Legendre, 2012; Peruzzetto et al., 2019), the most recent of which occurred in 1530 CE. Extensive hydrothermal alteration has been identified as having a key role in these events, based on the abundance of altered materials within the associated debris avalanche deposits (Komorowski et al., 2005; Le Friant et al., 2006; Salaün et al., 2011; Rosas-Carbajal et al., 2016; Peruzzetto et al., 2019; Heap et al., 2021a). The existence of hydrothermal fluid reservoirs (Brothelande et al., 2014; Rosas-Carbajal et al., 2016, 2017), perched aquifers (Lesparre et al., 2014), and the presence of listric-shaped, low-strength layers formed by the superposition of flank-collapse slip surfaces within and below the La Soufrière de Guadeloupe dome are anticipated to control the dynamics of future flank collapses and other mass-wasting phenomena (Rosas-Carbajal et al., 2016; Peruzzetto et al., 2019).

Meteoric fluid input is also significant at La Soufrière de Guadeloupe; for example, fumarole analysis by de Bremond d'Ars and Gibert (2022) highlights that meteoric input exerts an importance control on the otherwise seemingly stochastic dynamics of the shallow hydrothermal system. The volcano consistently receives over 5 m of rainfall annually at its summit (Dessert et al., 2015), with as much as 30% of meteoric input infiltrating into the

groundwater (Rad et al., 2007). As a result, frequent smaller mass-wasting events at La Soufrière de Guadeloupe have been directly related to intense rainfall events (Lesparre et al., 2014), including landslides concurrent with the passage of storms and hurricanes (Allemand et al., 2014); one such example is shown in Figure 1b. Very recently, parts of the *Chemin des Dames*, a tourist path on the west flank of the dome, required repair following small-volume, rain-induced landslides. This link between geohazards and the high-rainfall tropical climate echoes a broader trend of rainfall-induced hazards observed at volcanoes elsewhere in the Caribbean, including dome collapses (Matthews et al., 2002; Matthews and Barclay, 2004; Carn et al., 2004) and seismicity (Matthews et al., 2009). In a comparative analysis of global climate models, Farquharson and Amelung (2022) showed that models consistently project an increase in heavy rainfall across the volcanic areas of the Caribbean over the next eight decades. In Figure 1c, we plot projected change in heavy rainfall over La Soufrière de Guadeloupe obtained from the MRI-CGCM3 general circulation model of Japan's Meteorological Research Institute: clearly, the propensity for heavy rainfall events is set to increase in the near future (see also Cantet et al., 2014), even under the most ambitious climate change mitigation strategies (i.e. RCP 2.6).

Together, these factors highlight that La Soufrière de Guadeloupe represents an ideal natural laboratory to study the influence of water-saturation on the physical and mechanical properties of volcanic rock and volcano stability.

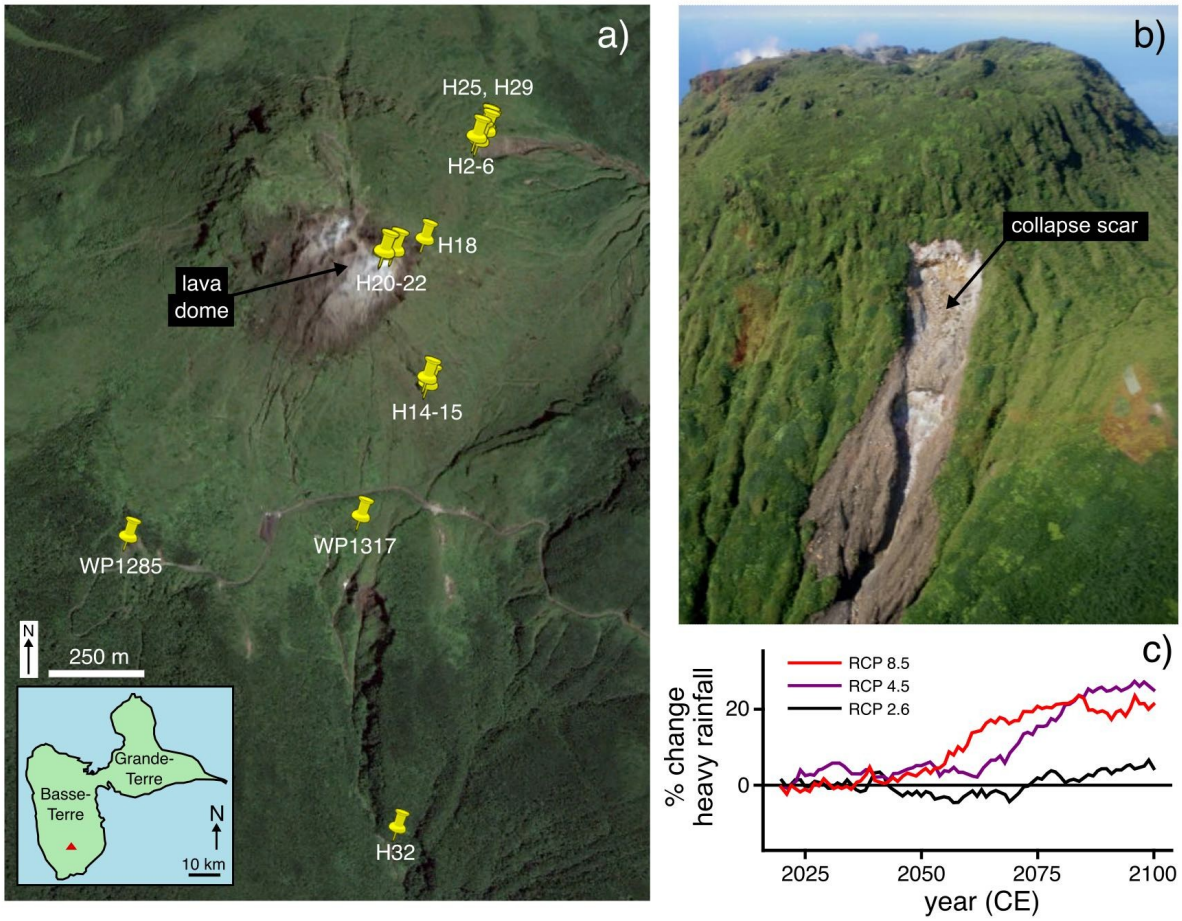

Figure 1. (a) Google Earth image (Google Maxar Technologies CNES / Airbus) of La Soufrière de Guadeloupe showing the sampling locations for the 17 rock blocks collected for this study. Inset shows a map of Guadeloupe in which the location of La Soufrière de Guadeloupe is indicated by a red triangle. (b) Photograph of the 2009 landslide scar on the northeastern flank of the dome (taken on 12 December 2009; photo credit: J.-B. de Chabalier, IPGP-OVSG). (c) Percentage change in heavy rainfall predicted for La Soufrière de Guadeloupe. Data are from the MRI-CGCM3 General Circulation Model results, provided by the Meteorological Research Institute, Japan, via the Earth System Grid Federation servers (https://esgf-node.llnl.gov/search/cmip5/). The change in projected heavy rainfall is resampled from monthly results corresponding to the 1.121 × 1.125 degree spatial grid containing La Soufrière de Guadeloupe, plotted as a function of time. For clarity, data are smoothed (15-year rolling mean) and normalised to 2023. Results are shown for three separate future

climate scenarios: a high emissions scenario (RCP 8.6), an intermediate emissions scenario (RCP 4.5), and a "very stringent" pathway, whereby global carbon dioxide emissions decrease to zero within 80 years (RCP 2.6). Further details are given in Farquharson and Amelung (2022).

3 Materials and Methods

3.1 Experimental materials

A suite of 17 variably altered andesite blocks from La Soufrière de Guadeloupe were used for this study (sampling locations are shown in Figure 1a). Eight of the 17 blocks were collected from a collapse scar to the northeast of dome summit (blocks H2A, H2B, H3, H4A, H5A, H6, H25, and H29). Four blocks were collected from the dome summit: one block from the wall of the Lacroix Supérieur outgassing fracture on the lava dome (H18), and three blocks from the lava spines that protrude the top of the current dome (one block from Cratère Sud Central, H20, and two blocks from an adjacent site, H21 and H22). A block was collected to the southwest of dome summit from a collapse scar into a highly fractured lava that forms the core of a paleo-collapse mega-block of the former volcanic edifice (WP1285). Blocks were also collected from the West wall of the fault "Faille du 30 août" on the lava dome (H14 and H15), and from a thick lava adjacent to the Galion waterfall (H32). The final block is a volcanic non-juvenile bomb from the dome that was ejected during the 1976–1977 explosive eruption (Komorowski et al., 2005) and landed on the roof of a small disused thermal bathhouse to the south of the dome summit (WP1317). We climbed on the roof of the bathhouse to collect the block.

These 17 blocks, previously described by Heap et al. (2021a, 2022a, b, c, 2023a, b), are porphyritic andesites characterised by a microcrystalline groundmass containing phenocrysts of dominantly plagioclase and pyroxene (orthopyroxene and clinopyroxene). The

mineral assemblage present in each block was identified by a combination of optical microscopy, Raman spectroscopy, and X-ray powder diffraction (XRPD), and quantitative phase analysis was performed using the XRPD data and the Rietveld approach (for more details see Heap et al., 2021a). The XRPD data show that all of the rocks contain variable quantities of secondary (alteration) minerals: kaolinite, alunite or natro-alunite, silica polymorphs (quartz, cristobalite, tridymite, and opal-A), hematite, pyrite, gypsum, and talc (Heap et al. 2021a, 2022a, b, c; Table 1). In this contribution, we quantify alteration as the wt % of secondary minerals in each block. The predominant hydrous alteration phases are kaolinite, natro-alunite, and opal-A (Table 1), suggesting fluid-rock interaction with acidic sulfate-chloride-rich fluids at relatively low temperatures (< 150–200 °C) (Inoue, 1995; Zimbelman et al., 2005; Scher et al., 2013; Fulignati, 2020; Heap et al., 2021a).

Mineral	H2A	H2B	H3	H4A	H5A	H6	H14	H15	H18	H20	H21	H22	H25	H29	H32	WP1285	WP1317
Plagioclase	56.7	12.3	46.6	23.3	41.3	30.0	60.7	22.5	61.2	28.7	24.2	59.5	38.7	62.4	64.4	64.7	61.6
Clinopyroxene	8.7	3.4	5.6	4.9	5.2	6.4	6.3	7.3	8.4	8.9	12.4	8.9	5.3	7.8	9.5	5.2	5.9
Orthopyroxene	10.8	9.5	11.8	11.8	11.1	10.8	8.6	9.2	12.2	15.0	19.3	13.6	10.2	11.2	15.1	13.2	15.6
(Ti-) Magnetite	0.7	-	0.8	-	-	-	0.8	-	2.9	2.4	3.1	0.8	-	2.7	4.9	3.5	0.7
Quartz*	1.0	0.5	0.6	0.6	0.5	0.5	1.7	0.7	0.7	0.3	0.2	0.6	0.3	0.4	0.3	0.2	0.7
Cristobalite*	11.3	12.8	10.6	11.8	13.0	11.1	13.5	10.2	11.7	11.4	11.7	10.6	9.8	12.4	5.7	-	-
Tridymite*	-	-	-	-	-	-	-	0.7	-	-	-	-	-	-	-	13.2	13.2
Hematite*	-	-	-	-	-	-	3.4	-	2.8	-	-	-	-	3.1	-	-	-
Pyrite*	3.5	-	3.8	2.3	-	-	-	-	-	-	0.4	3.1	0.6	-	-	-	-
Alunite*	-	-	-	-	-	-	-	-	-	-	-	-	-	-	-	-	2.4
Na-Alunite*	1.4	1.6	2.8	1.3	5.4	5.1	5.1	15.0	-	0.5	0.5	-	9.8	-	-	-	-
Gypsum*	-	-	-	0.7	-	-	-	-	-	0.8	1.2	-	-	-	-	-	-
Kaolinite*	6	59.7	17.4	43.3	23.5	36.0	< 1	34.3	-	2.0	2.0	< 1	25.3	-	-	-	-
Talc*	-	-	-	-	-	-	-	-	-	-	-	2.9	-	-	-	-	-
Opal-A*	-	-	-	-	-	-	-	-	-	30	25	-	-	-	-	-	-

Table 1. Mineral contents of the 17 rock blocks from La Soufrière de Guadeloupe measured by X-ray powder diffraction. Values in wt%. Asterisk denotes a secondary mineral (i.e. alteration mineral). Data from Heap et al. (2021a, 2022a, b, c). The relative uncertainties in the quantification are in the order of 5–10%. Sample locations are provided in Figure 1a.

3.2 Experimental methods

Cylindrical samples were prepared from each of the blocks to a diameter of 20 mm and then cut and precision-ground to a nominal length of 40 mm. The cylindrical samples

cored from a particular block were assumed to have the same mineral contents as the parent block (i.e. those listed in Table 1). The samples were first washed using tapwater and then dried in a vacuum-oven at 40 °C for at least 48 h. The connected porosity of all the samples was calculated using the bulk sample volume and the skeletal (solid) sample volume of the oven-dry samples measured by a helium pycnometer. Relative uncertainties of measurements of connected porosity are < 2%.

Dry uniaxial compressive strength was measured on multiple oven-dry samples from all 17 blocks in a uniaxial load frame located in the laboratory at the Strasbourg Institute of Earth & Environment (ITES, France) (Figure 2a). Samples were deformed under ambient laboratory pressure and temperature at a constant axial strain rate of 10^{-5} s^{-1} until macroscopic failure. Axial displacement and axial load were measured using a linear variable differential transducer and a load cell, respectively. Axial displacement (minus the displacement accumulated within the load chain) and axial load were converted to axial strain and axial stress using the sample dimensions. Relative uncertainties of measurements of uniaxial compressive strength are < 1%. The static Young's modulus was determined from the elastic portion of the uniaxial stress-strain curves (Heap et al., 2020a). Relative uncertainties of measurements of Young's modulus are < 2%. The uniaxial compressive strength and Young's modulus of the samples deformed dry were previously published in Heap et al. (2021a) (with the exception of samples from block H32).

Water-saturated (wet) uniaxial compressive strength, data unique to this contribution, was measured on multiple samples from all 17 blocks using the same uniaxial load frame, inside a water bath (Figure 2b). The samples to be deformed under saturated conditions were specifically selected so that their appearance and connected porosity was the same, or very similar, to the samples deformed under dry conditions from the same block (so that their dry and wet uniaxial compressive strength and Young's modulus can be compared directly). To do

so, multiple samples were prepared from each block and only those with a similar appearance and porosity were selected for experimentation. Using this approach, the porosity difference between each sample pair was in the range 0.00–0.03, which we consider to be sufficient to allow for direct comparisons between the dry and wet uniaxial compressive strength and Young's modulus of each of the blocks. Prior to deformation, the samples were vacuum-saturated in de-aired, deionised water. The water-saturation procedure was as follows. (1) The samples were placed inside a glass container, which was then placed within a bell jar. (2) The samples were vacuumed inside the bell jar for at least 12 h at room temperature. (3) Maintaining the vacuum inside the bell jar, de-aired, deionised water was introduced into the glass container until the samples were completely submerged. (4) The samples were left submerged within the vacuumed bell jar for at least 6 h, after which the vacuum was released and the glass container containing the samples was removed from the bell jar. (5) The samples remained submerged in de-aired, deionised water until deformed. As for the dry experiments, the static Young's modulus was then determined from the elastic portion of the uniaxial stress-strain curves. Samples from block H32, too strong to measure in the uniaxial load frame at the ITES, were measured at the Laboratory of Experimental Rock Mechanics at the Ecole Polytechnique Fédérale de Lausanne (EPFL, Switzerland) using a similar uniaxial setup. We consider the dry samples deformed in Heap et al. (2021a) to have a water saturation of 0%, and the wet samples deformed herein to have a water saturation of 100%.

Although rock strength and Young's modulus will increase as a function of pressure (or depth) in the brittle regime, we highlight that lava domes are typically only a few hundred metres high (the lava dome at La Soufrière de Guadeloupe, for example, is about 250–300 m high) and that rock physical and mechanical properties (e.g., uniaxial compressive strength and Young's modulus) will not change significantly under pressures representative of a depth of a few hundred metres.

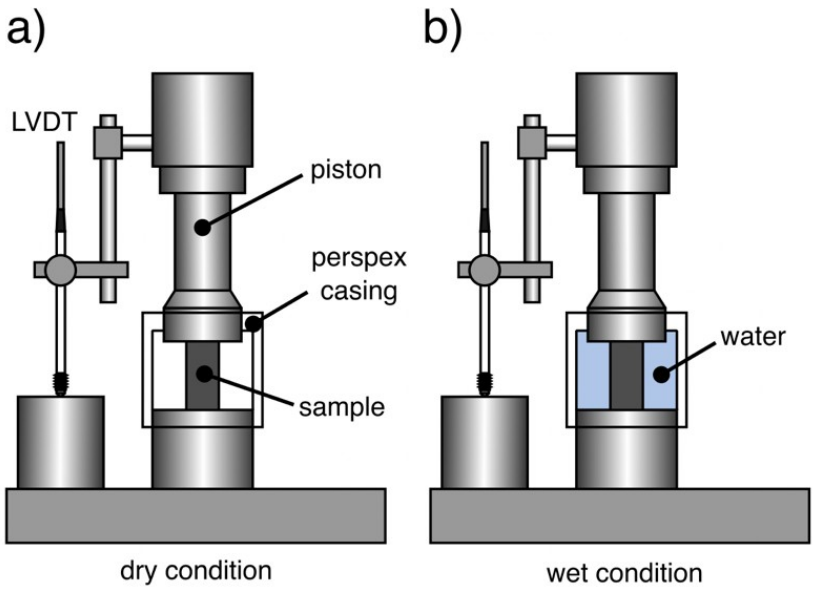

Figure 2. Schematic diagrams of the uniaxial compression apparatus at the Strasbourg Institute of Earth & Environment (ITES). (a) Setup for the dry experiments. (b) Setup for the wet experiments.

3.3 Numerical modelling

To explore the effect of water-saturation on dome stability, we used 2D Discrete Element Method (DEM) models created in Particle Flow Code (PFC; Itasca Consulting Group Ltd), following the methods outlined by Harnett et al. (2018) and Harnett and Heap (2021). PFC has been previously used to successfully model the mechanical behaviour of rock (e.g., Potyondy and Cundall, 2004) and, recently, to model dome growth and collapse (Husain et al., 2014, 2018; Harnett et al., 2018; Husain et al., 2019; Harnett and Heap, 2021; Harnett et al., 2022; Walter et al., 2022; Heap et al., 2023a). These DEM models consider a particle-based material in which circular particles interact at interparticle contacts. Contact behaviour is primarily governed by stiffness and cohesion. At the boundary between the particles and walls (i.e. the ground surface), the contact behaviour is cohesionless and governed by friction.

313 The particle size in the model is not representative of individual crystals, grains, or rock
314 blocks, but rather represents discretisation of the medium for the purpose of computation.
315 First, we numerically generated two fully solid domes (see Harnett and Heap, 2021)
316 containing 9745 circular particles and 22710 contacts. The contact properties were guided by
317 our experimental data for dry unaltered and altered dome rocks (uniaxial compressive
318 strength, tensile strength, and Young's modulus). An iterative calibration procedure was
319 required to relate contact parameters to bulk rock parameters, whereby uniaxial compression
320 tests are reproduced in PFC (see Harnett and Heap (2021) for details). Using these calibrated
321 parameters, we created initially stable dry unaltered and altered domes. These stable domes
322 will not deform unless perturbed in some way. To explore the effect of water-saturation on the
323 stability of these domes, we modified the mechanical properties of the contacts in the domes
324 to represent wet unaltered and altered dome rocks, also guided by our experimental data. The
325 model then provided the displacement within the dome resulting from water-saturation.
326 Finally, we generated another initially stable fully solid dome using properties representative
327 of dry unaltered rock. In the first scenario, we perturbed the dome by including a dry altered
328 zone within the dome (as in Harnett et al., 2022). In the second scenario, we also included the
329 buried altered zone within the dome, but, instead, we used properties representative of wet
330 unaltered and altered rock. We highlight that, although we use properties representative of
331 uniaxial conditions in our models and, therefore, we do not explicitly consider an increase in
332 strength with depth in the model, the models have an inherent depth-dependence of
333 mechanical properties through the inclusion of gravity: the contact forces at the base of the
334 dome are much higher than those at the surface of the dome. Further, as mentioned above, we
335 also do not expect rock physical and mechanical properties (e.g., uniaxial compressive
336 strength and Young's modulus) to change significantly under pressures representative of a
337 depth of a few hundred metres. For the modelling of much larger, or deeper, features, we

recommend that triaxial deformation experiments are performed to understand how rock physical and mechanical properties evolve as a function of pressure (depth).

4 Results

Representative uniaxial stress-strain curves for dry and wet samples are shown in Figure 3 (for block H6). We highlight that the connected porosity of the dry and wet H6 samples shown in Figure 3 is 0.18 and 0.16, respectively (Table 2). These curves show that the uniaxial compressive strength and the Young's modulus (the slope of the stress-strain curve in the pseudo-linear elastic regime) are lower when the sample is wet. We also note that the axial strain at the peak stress is slightly lower for the wet sample than for the dry sample (Figure 3).

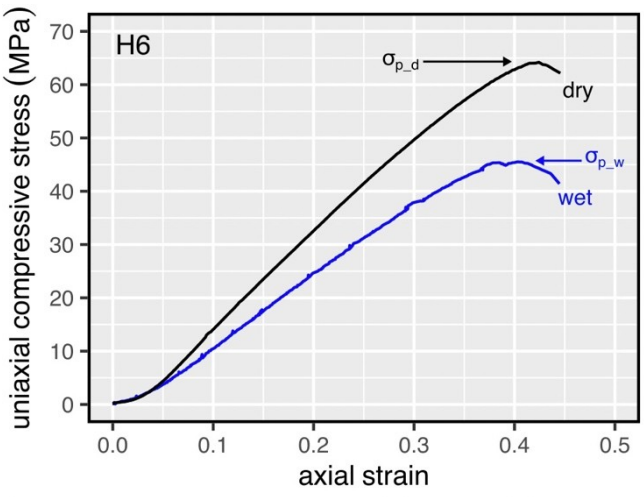

Figure 3. Representative stress-strain curves for dry (black curve) and wet (blue curve) samples from block H6 from La Soufrière de Guadeloupe (Eastern Caribbean). The dry, σ_{p_d}, and wet, σ_{p_w}, uniaxial compressive strengths are indicated on the curves.

Dry (black circles) and wet (blue squares) uniaxial compressive strength data are plotted as a function of connected porosity and the wt% of secondary minerals in Figures 4a

and 4b, respectively (data available in Table 2). These data show that uniaxial compressive strength decreases as a function of connected porosity and the wt% of secondary minerals. For example, strength decreased from ~270 MPa to only a couple of MPa as porosity decreased from ~0.05 to > 0.4 (Figure 4a). These data also show that, for a given porosity, the strength of wet samples is typically lower than the strength of dry samples. Block H2B (porosity ~0.45; alteration 75 wt%; Table 2) and block H2A (porosity ~0.18; alteration 23 wt%) are characterised by the lowest and highest ratio of wet to dry strength, respectively.

We also show dry (black circles) and wet (blue squares) Young's modulus as a function of connected porosity and the wt% of secondary minerals in Figures 4c and 4d, respectively (data available in Table 2). Similar to the strength data of Figure 4a and 4b, the data of Figure 4c and 4d show that (1) Young's modulus decreases as a function of connected porosity and the wt% of secondary minerals and (2) for a given porosity, the Young's modulus of wet samples is typically lower than the Young's modulus of dry samples. For example, Young's modulus decreased from ~40 GPa to only a couple of GPa as porosity increases from ~0.05 to > 0.4 (Figure 4c) or as the wt% of secondary minerals increases from ~15 to ~75 wt% (Figure 4d). Block H2B (porosity ~0.45; alteration 75 wt%; Table 2) and block WP1317 (porosity ~0.14; alteration 16 wt%) are characterised by the lowest and highest ratio of wet to dry Young's modulus, respectively.

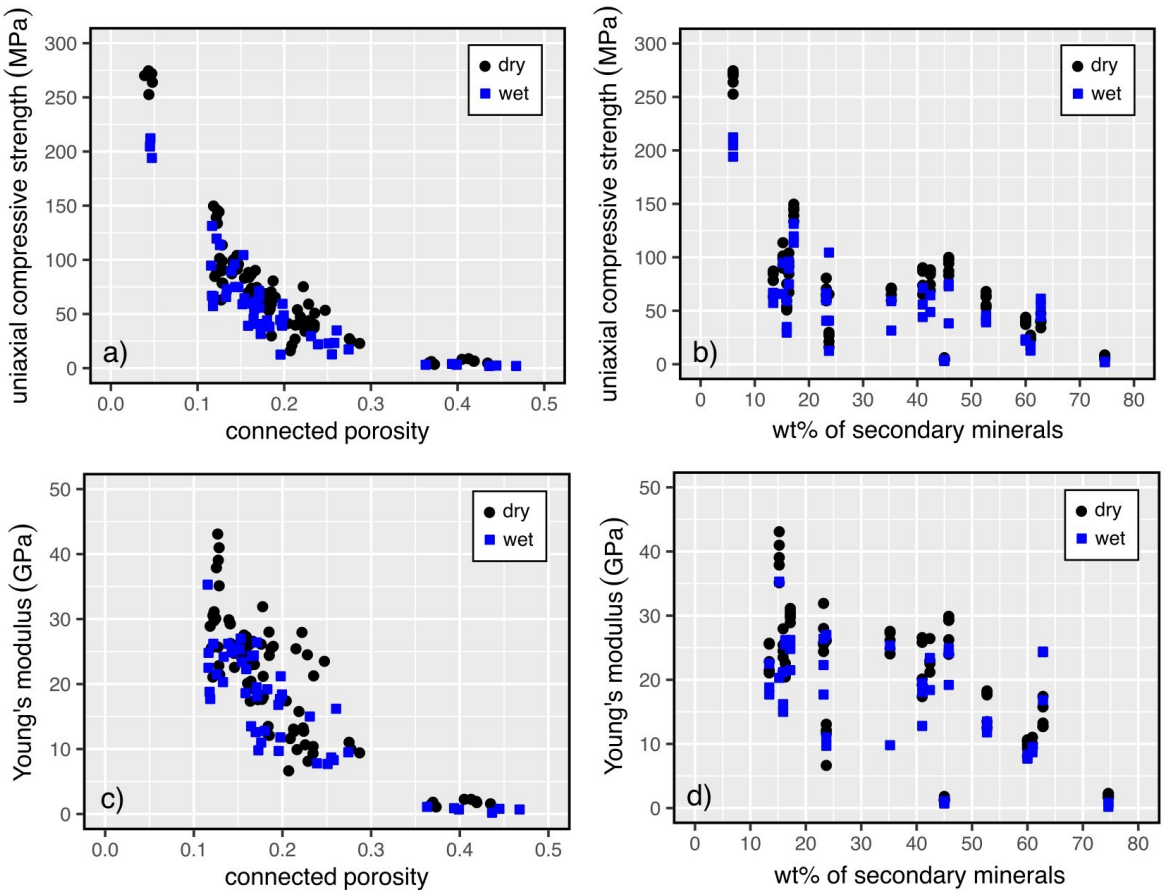

376

377 **Figure 4.** Uniaxial compressive strength of dry (black circles) and wet (blue squares) samples
378 from La Soufrière de Guadeloupe (Eastern Caribbean) as a function of (a) connected porosity
379 and (b) the wt% of secondary minerals. Young's modulus of dry and wet samples from La
380 Soufrière de Guadeloupe as a function of (c) connected porosity and (d) the wt% of secondary
381 minerals. Dry data (apart from data for H32) are from Heap et al. (2021a). The relative
382 uncertainties of the connected porosity, uniaxial compressive strength, and Young's modulus
383 are < 2%, < 1%, and < 2%, respectively; the uncertainties are therefore captured by the
384 symbol size. The relative uncertainties in the quantification of the mineral contents (Table 1)
385 are on the order of 5–10%.

386

387 To better highlight the difference between wet and dry strength and Young's modulus,
388 the ratio of wet to dry strength and the ratio of wet to dry Young's modulus are plotted as a

function of connected porosity and the wt% of secondary minerals in Figure 5 (data available in Table 3). This ratio is obtained by organising the samples from the same block deformed under dry and wet conditions into pairs, and then dividing the data for the sample deformed under saturated conditions with the data for their corresponding dry counterpart. As mentioned above, the samples deformed under saturated conditions were specifically selected so that their appearance and porosities were the same, or very similar, to those deformed under dry conditions. A ratio of one therefore corresponds to the scenario in which the dry and wet properties are exactly the same, and a ratio below and above one indicates that the sample property is lower or higher when wet, respectively. Figure 5a shows that all of the samples have a wet to dry strength lower than one, indicating that all samples were weaker when saturated with water. These data also show that the wet to dry strength ratio appears to decrease as a function of increasing porosity (Figure 5a) and wt% of secondary minerals (Figure 5b). Figure 5c shows that the majority of the samples have a wet to dry Young's modulus ratio below one. Although the wet to dry Young's modulus ratio appears to decrease as a function of increasing porosity (Figure 5c), there appears to be no discernible trend as a function of increasing wt% of secondary minerals (Figure 5d), although we highlight that the samples with the lowest wet to dry Young's modulus ratio contain the highest proportion of secondary minerals (Figure 5d).

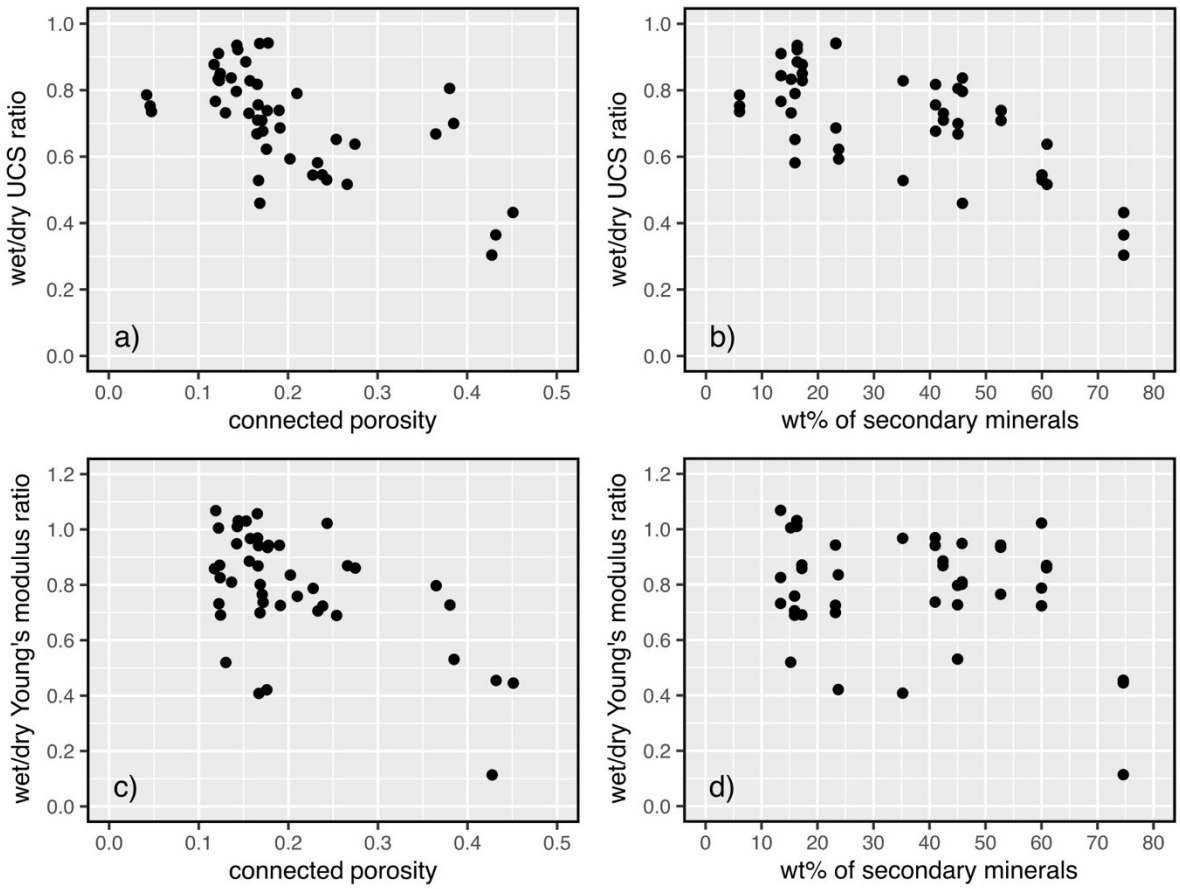

Figure 5. Ratio of wet to dry uniaxial compressive strength (UCS) for samples from La Soufrière de Guadeloupe (Eastern Caribbean) as a function of (a) connected porosity and (b) the wt% of secondary minerals. Ratio of wet to dry Young's modulus for samples from La Soufrière de Guadeloupe as a function of (c) connected porosity and (d) the wt% of secondary minerals. The relative uncertainties of the connected porosity, uniaxial compressive strength, and Young's modulus are < 2%, < 1%, and < 2%, respectively; the uncertainties are therefore captured by the symbol size. The relative uncertainties in the quantification of the mineral contents (Table 1) are on the order of 5–10%.

Sample	Weight percentage of secondary minerals	Connected porosity	Condition	Uniaxial compressive strength (MPa)	Young's modulus (GPa)
H2A_2	23	0.18	Dry	63.7	31.9
H2A_5	23	0.19	Dry	80.5	25.5
H2A_6	23	0.19	Dry	65.4	25.8
H2A_11	23	0.19	Dry	59.3	24.4

H2A_12	23	0.18	Dry	70.4	28.0
H2A_7	23	0.17	Wet	66.3	26.4
H2A_10	23	0.16	Wet	59.9	22.3
H2A_14	23	0.20	Wet	40.7	17.7
H2B_3	75	0.42	Dry	6.6	1.8
H2B_10	75	0.42	Dry	6.4	1.9
H2B_11	75	0.41	Dry	8.7	2.3
H2B_12	75	0.41	Dry	8.1	2.3
H2B_15	75	0.43	Dry	4.6	1.6
H2B_7	75	0.44	Wet	2.0	0.2
H2B_9	75	0.47	Wet	2.0	0.7
H2B_13	75	0.44	Wet	2.4	0.8
H3_3	35	0.16	Dry	70.3	27.3
H3_7	35	0.16	Dry	69.9	24.9
H3_8	35	0.16	Dry	64.8	27.5
H3_11	35	0.16	Dry	59.7	24.0
H3_13	35	0.16	Dry	71.2	26.2
H3_14	35	0.17	Wet	31.5	9.8
H3_15	35	0.15	Wet	59.0	25.3
H4A_2	60	0.23	Dry	40.3	10.4
H4A_4	60	0.23	Dry	42.0	10.6
H4A_6	60	0.23	Dry	43.9	8.1
H4A_8	60	0.23	Dry	37.2	9.3
H4A_9	60	0.22	Dry	40.4	9.9
H4A_5	60	0.25	Wet	22.9	.7.7
H4A_7	60	0.26	Wet	23.3	8.3
H4A_10	60	0.24	Wet	22.0	7.8
H5A_2	42	0.16	Dry	88.3	26.4
H5A_3	42	0.16	Dry	86.6	22.8
H5A_5	42	0.16	Dry	83.9	22.5
H5A_8	42	0.18	Dry	68.8	21.2
H5A_10	42	0.17	Dry	74.5	23.0
H5A_4	42	0.20	Wet	48.8	18.4
H5A_9	42	0.15	Wet	64.5	23.4
H6_6	53	0.18	Dry	55.1	13.5
H6_9	53	0.18	Dry	68.0	18.0
H6_9	53	0.18	Dry	53.0	12.5
H6_12	53	0.18	Dry	64.2	17.6
H6_13	53	0.18	Dry	63.0	18.3
H6_2	53	0.16	Wet	45.5	13.5
H6_3	53	0.20	Wet	39.2	11.8
H6_5	53	0.17	Wet	40.7	12.6
H14_2	24	0.18	Dry	65.4	26.1
H14_3	24	0.21	Dry	21.1	11.6
H14_5	24	0.21	Dry	26.8	13.1
H14_6	24	0.19	Dry	29.8	12.1
H14_10	24	0.21	Dry	16.1	6.6
H14_8	24	0.20	Wet	12.5	9.7
H14_11	24	0.18	Wet	40.7	11.0
H15_3	61	0.28	Dry	24.6	10.0
H15_4	61	0.28	Dry	27.1	11.0
H15_5	61	0.29	Dry	22.8	9.4
H15_6	61	0.27	Wet	17.3	9.5
H15_7	61	0.25	Wet	12.7	8.7
H18_3	15	0.13	Dry	101.3	37.9
H18_4	15	0.13	Dry	89.8	39.1
H18_5	15	0.13	Dry	98.8	41.0
H18_6	15	0.13	Dry	93.2	43.1

H18_7	15	0.13	Dry	113.7	35.1
H18_11	15	0.13	Wet	65.7	20.3
H18_14	15	0.12	Wet	94.7	35.3
H20_2	45	0.37	Dry	4.8	1.2
H20_3	45	0.37	Dry	4.4	1.3
H20_7	45	0.37	Dry	4.6	1.4
H20_8	45	0.37	Dry	6.1	1.8
H20_10	45	0.37	Dry	3.4	1.1
H20_5	45	0.39	Wet	3.9	0.9
H20_6	45	0.40	Wet	3.1	0.7
H20_11	45	0.36	Wet	3.1	1.1
H21_3	41	0.17	Dry	90.2	26.6
H21_8	41	0.16	Dry	65.2	17.4
H21_11	41	0.16	Dry	86.9	25.8
H21_12	41	0.16	Dry	73.8	19.2
H21_13	41	0.16	Dry	87.2	20.1
H21_4	41	0.17	Wet	71.3	19.5
H21_6	41	0.18	Wet	44.1	12.8
H21_15	41	0.17	Wet	55.8	18.1
H22_2	17	0.12	Dry	145.7	29.7
H22_3	17	0.12	Dry	144.3	30.1
H22_4	17	0.12	Dry	139.1	30.5
H22_5	17	0.12	Dry	149.7	28.9
H22_6	17	0.12	Dry	133.6	31.1
H22_7	17	0.12	Wet	119.6	26.2
H22_14	17	0.12	Wet	131.3	24.8
H22_15	17	0.13	Wet	113.6	21.5
H25_2	46	0.14	Dry	99.9	29.3
H25_4	46	0.14	Dry	97.7	29.3
H25_5	46	0.14	Dry	94.2	26.2
H25_9	46	0.14	Dry	87.1	29.9
H25_12	46	0.15	Dry	83.1	24.0
H25_3	46	0.18	Wet	38.2	19.2
H25_10	46	0.13	Wet	72.9	24.2
H25_14	46	0.14	Wet	75.0	24.9
H29_2	16	0.22	Dry	53.9	25.4
H29_8	16	0.23	Dry	59.1	24.5
H29_9	16	0.22	Dry	75.2	27.9
H29_12	16	0.25	Dry	53.4	23.5
H29_16	16	0.24	Dry	50.7	21.3
H29_3	16	0.20	Wet	59.4	21.2
H29_6	16	0.26	Wet	34.8	24.2
H29_13	16	0.23	Wet	29.5	24.9
H32_1	6	0.04	Dry	270.1	-
H32_4	6	0.05	Dry	263.9	-
H32_5	6	0.05	Dry	271.9	-
H32_6	6	0.04	Dry	274.5	-
H32_7	6	0.04	Dry	252.6	-
H32_8	6	0.05	Wet	194.1	-
H32_9	6	0.05	Wet	204.6	-
H32_10	6	0.04	Wet	212.2	-
WP1285_2	13	0.13	Dry	78.5	22.8
WP1285_8	13	0.13	Dry	63.0	25.7
WP1285_10	13	0.13	Dry	78.3	21.4
WP1285_11	13	0.12	Dry	87.2	21.1
WP1285_15	13	0.12	Dry	84.6	25.6
WP1285_4	13	0.12	Wet	66.1	17.7
WP1285_6	13	0.12	Wet	57.3	18.8

WP1285_9	13	0.12	Wet	66.8	22.5
WP1317_2	16	0.16	Dry	67.3	20.4
WP1317_6	16	0.16	Dry	84.5	24.7
WP1317_7	16	0.15	Dry	91.5	22.6
WP1317_8	16	0.15	Dry	95.8	25.9
WP1317_12	16	0.15	Dry	104.0	24.7
WP1317_10	16	0.15	Wet	74.8	25.5
WP1317_13	16	0.14	Wet	89.6	26.2
WP1317_15	16	0.14	Wet	95.9	25.5

418

419 **Table 2**. Experimental condition (dry or wet), connected porosity, uniaxial compressive
420 strength, Young's modulus, and the percentage of secondary minerals (i.e. alteration) for the
421 samples prepared for this study. Sample locations are provided in Figure 1a. Dry data (apart
422 from data for H32) are from Heap et al. (2021a). The relative uncertainties of the connected
423 porosity, uniaxial compressive strength, and Young's modulus are < 2%, < 1%, and < 2%,
424 respectively. The relative uncertainties in the quantification of the mineral contents (Table 1)
425 are on the order of 5–10%.

426

Sample	Weight percentage of secondary minerals	Connected porosity	wet/dry UCS ratio	wet/dry Young's modulus ratio
H2A	23	0.17	0.94	0.70
H2A	23	0.18	0.94	0.94
H2A	23	0.19	0.69	0.73
H2B	75	0.45	0.43	0.45
H2B	75	0.43	0.30	0.11
H2B	75	0.43	0.36	0.45
H3	35	0.17	0.53	0.41
H3	35	0.16	0.83	0.97
H4A	60	0.23	0.54	0.79
H4A	60	0.24	0.55	0.72
H4A	60	0.24	0.53	1.02
H5A	42	0.16	0.73	0.89
H5A	42	0.17	0.71	0.87
H6	53	0.17	0.71	0.77
H6	53	0.19	0.74	0.94
H6	53	0.18	0.74	0.93
H14	24	0.20	0.59	0.84
H14	24	0.18	0.62	0.42
H15	61	0.27	0.64	0.86
H15	61	0.27	0.52	0.87
H18	15	0.12	0.83	1.01
H18	15	0.13	0.73	0.52
H20	45	0.38	0.81	0.73
H20	45	0.38	0.70	0.53

H20	45	0.36	0.67	0.80
H21	41	0.17	0.82	0.97
H21	41	0.17	0.68	0.74
H21	41	0.17	0.76	0.94
H22	17	0.12	0.85	0.69
H22	17	0.12	0.88	0.86
H22	17	0.12	0.83	0.87
H25	46	0.14	0.80	0.95
H25	46	0.14	0.84	0.81
H25	46	0.17	0.46	0.80
H29	16	0.21	0.79	0.76
H29	16	0.25	0.65	0.69
H29	16	0.23	0.58	0.71
H32	6	0.05	0.74	-
H32	6	0.05	0.75	-
H32	6	0.04	0.79	-
WP1285	13	0.12	0.77	1.07
WP1285	13	0.12	0.91	0.73
WP1285	13	0.12	0.84	0.83
WP1317	16	0.14	0.92	1.03
WP1317	16	0.14	0.93	1.01
WP1317	16	0.15	0.89	1.03

Table 3. Percentage of secondary minerals (i.e. alteration), average connected porosity, the ratio of wet to dry uniaxial compressive strength, and the ratio of wet to dry Young's modulus for the samples prepared for this study. Sample locations are provided in Figure 1a. The relative uncertainties of the connected porosity, uniaxial compressive strength, and Young's modulus are < 2%, < 1%, and < 2%, respectively. The relative uncertainties in the quantification of the mineral contents (Table 1) are on the order of 5–10%.

5 Discussion

5.1 Water-weakening in volcanic rocks: the influence of porosity

Our data show that the uniaxial compressive strength and Young's modulus of variably-altered dome lavas from La Soufrière de Guadeloupe are reduced when water-saturated (Figures 4 and 5), in agreement with previous studies on volcanic rocks (Zhu et al., 2011; Heap et al., 2015; Zhu et al., 2016; Heap et al., 2018; Kendrick et al., 2021; Heap and Violay, 2021).

We plot the ratio of wet to dry strength and the ratio of wet to dry Young's modulus as a function of connected porosity for our new data alongside published data for volcanic rocks in Figures 6a and 6b, respectively. Figures 6a and 6b show that, based on previously published data for andesite, basalt, dacite, and welded block-and-ash flow, one would conclude that water-weakening in volcanic rocks does not appear to vary systematically with porosity. Previous studies have also shown that porosity does not appear to influence water-weakening in sandstones (Heap et al., 2019), limestones (Baud et al., 2016), and tuffs (Zhu et al., 2011; Heap et al., 2018; Frolova et al., 2021). Our new data for hydrothermally altered andesites from La Soufrière de Guadeloupe, however, suggest that porosity exerts influence on their water-weakening behaviour (Figures 6a and 6b). This may be because the porosity range studied in previous contributions was insufficient to observe a trend (the most porous sample from the previously published dataset is a dacite with a porosity of ~0.3, whereas the maximum porosity in our dataset is ~0.45; Figures 6 and 6b). Although we conclude that porosity appears to exert influence on water-weaking in our sample suite, we suggest that more data for high-porosity volcanic rocks are now required to make firm conclusions as to the influence of porosity on water-weakening in volcanic rocks (based on reasoning discussed in the next subsection).

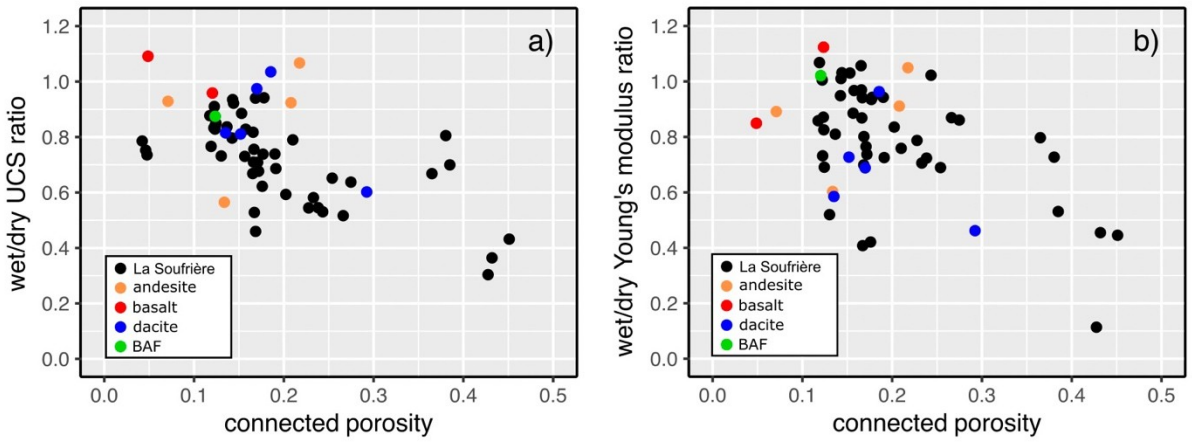

Figure 6. Ratio of wet to dry (a) uniaxial compressive strength and (b) Young's modulus for samples from La Soufrière de Guadeloupe (Eastern Caribbean) as a function of connected porosity (black circles). Data for andesite (orange circles), basalt (red circles), and block-and-ash flow (BAF; green circles) from Heap and Violay (2021). Data for dacite (blue circles) from Kendrick et al. (2021). For the data for the samples from La Soufrière de Guadeloupe, the relative uncertainties of the connected porosity, uniaxial compressive strength, and Young's modulus are < 2%, < 1%, and < 2%, respectively; the uncertainties are therefore captured by the symbol size.

5.2 Water-weakening in volcanic rocks: the influence of alteration

We first note that the uniaxial compressive strength (Figure 4b) and Young's modulus (Figure 4d) of water-saturated andesites from La Soufrière de Guadeloupe are reduced as a function of increasing wt% of secondary minerals. Previously, hydrothermal alteration has been shown to either decrease (e.g., Frolova et al., 2014; Pola et al., 2014; Wyering et al., 2014; Mordensky et al., 2018, 2019; Heap et al., 2021a; Darmawan et al., 2022; Schaefer et al., 2023) or increase the strength of volcanic rocks (e.g., Frolova et al., 2014; Pola et al., 2014; Wyering et al., 2014; Coats et al., 2018; Heap et al., 2020b, 2021b). These studies, and others, have shown that whether or not hydrothermal alteration decreases or increases strength depends on the type of alteration and/or whether the alteration results in increases or decreases to porosity.

In the case of hydrothermally altered dome rocks from La Soufrière de Guadeloupe, Heap et al. (2021a, 2022) concluded that alteration had reduced their uniaxial compressive strength and Young's modulus. However, these authors also noted that there is a relationship between porosity and alteration (Figure 7). As discussed by these authors, it is difficult to unravel the influence of porosity and alteration on the strength of these materials because it is

unclear whether alteration increased the porosity of the samples or whether the more porous samples are more altered due to their higher fluid-rock ratios. However, based on the presence of abundant clays and dissolution textures in these samples, Heap et al. (2021a, 2022) concluded uniaxial compressive strength and Young's modulus were likely reduced by hydrothermal alteration. We conclude the same here, although we highlight that the main focus of this contribution is to study the influence of water-saturation on the mechanical properties of hydrothermally altered dome rocks, discussed below.

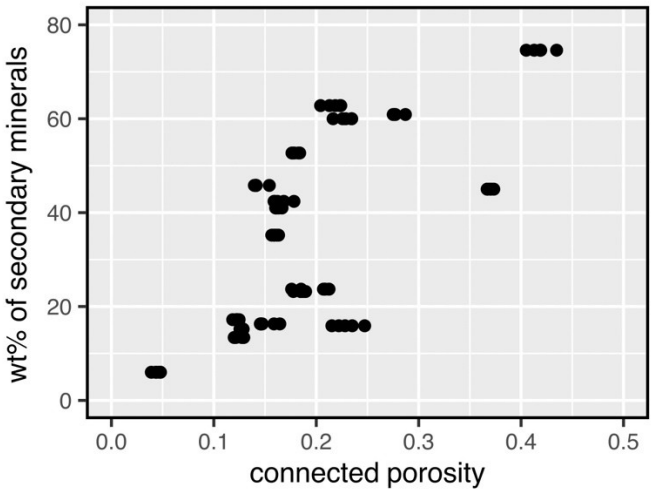

Figure 7. The wt% of secondary minerals as a function of connected porosity for samples from La Soufrière de Guadeloupe (Eastern Caribbean).

Our data suggest that the wet to dry strength ratio decreases as a function of increasing wt% of secondary minerals (Figure 5b), although there appears to be no discernible trend in the wet to dry Young's modulus ratio as a function of increasing wt% of secondary minerals (Figure 5d). In other words, these data suggest that the reduction in strength due to the presence of water increases as a function of the degree of hydrothermal alteration and, therefore, the abundance of secondary (alteration) minerals. These results are in agreement with the previous laboratory data for tuff, which suggest that the presence of alunite (Heap et

al., 2015) and zeolites and clay minerals (Heap et al., 2018) may be responsible for the reduction in uniaxial compressive strength in the presence of water. Expansive clay minerals, for example, can mechanically degrade as a function of increasing water content (Nara et al., 2012). The fact that alteration increases the observed water-weakening (Figure 5b) and that alteration increases as a function of connected porosity for these rocks (Figure 7) also suggests that the observed trends as a function of porosity (Figures 6a and 6b) could be because the high-porosity rocks are more altered, and it is the alteration that is dictating the observed water-weakening. As stated above, more experiments are now required to make firm conclusions as to the influence of porosity on water-weakening in volcanic rocks.

To further investigate the influence of alteration on water-weakening, we replot the ratio of wet to dry uniaxial compressive strength and Young's modulus as a function of a subset of the alteration minerals (alunite, Na-alunite, gypsum, kaolinite, and talc only; i.e. excluding cristobalite, tridymite, hematite, pyrite, and opal-A) in Figure 8. We include those minerals that have previously been considered to reduce the strength of rock upon water-saturation. We highlight that the coefficients of determination for simple linear fits to the data shown in Figure 8 are very similar to those for the data shown in Figures 5b and 5d. Therefore, these data suggest that the selected alteration minerals (alunite, Na-alunite, gypsum, kaolinite, and talc) are likely those influencing the uniaxial compressive strength of these rocks in the presence of water (Figure 8a).

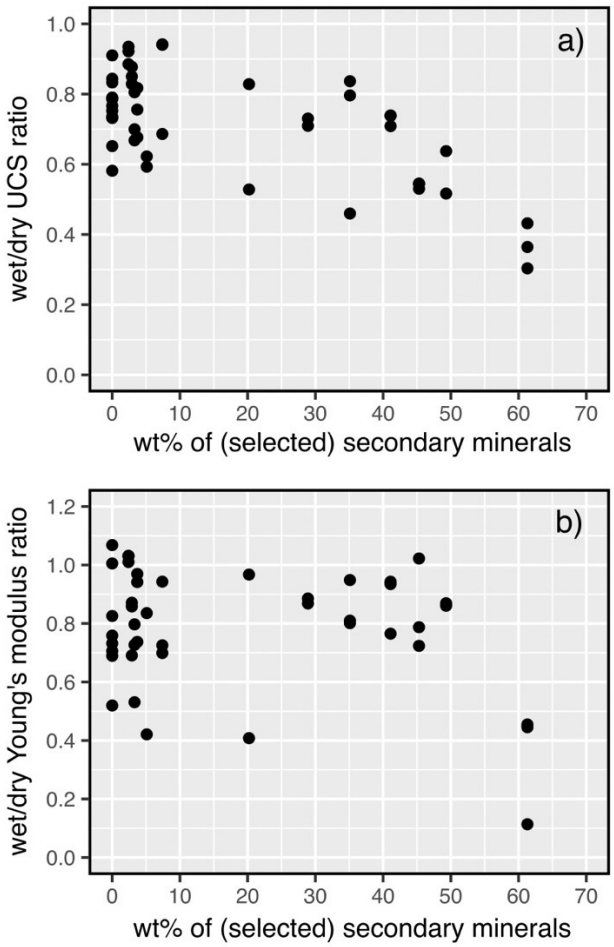

525

526 **Figure 8.** Ratio of wet to dry (a) uniaxial compressive strength and (b) Young's modulus as a
527 function of the wt% of a subset of the secondary minerals for samples from La Soufrière de
528 Guadeloupe (Eastern Caribbean). The alteration minerals included are alunite, Na-alunite,
529 gypsum, kaolinite, and talc only (i.e. excluding cristobalite, tridymite, hematite, pyrite, and
530 opal-A). The relative uncertainties of the uniaxial compressive strength and Young's modulus
531 are < 1% and < 2%, respectively; the uncertainties are therefore captured by the symbol size.
532 The relative uncertainties in the quantification of the mineral contents (Table 1) are on the
533 order of 5–10%.

534

535 To investigate the mechanism responsible for the observed weakening in the presence
536 of water, and the increase in water-weakening as a function of alteration (Figures 4b, 5b, and

537 8a), we use the analytical approximation of Sammis and Ashby's (1986) pore-emanating crack
538 micromechanical model provided by Zhu et al. (2010):
539
540 $$UCS = \frac{1.325}{\phi^{0.414}} \frac{K_{IC}}{\sqrt{\pi r}} \quad (1).$$
541
542 The pore-emanating crack model of Sammis and Ashby (1986) has been widely used to
543 investigate the mechanical behaviour of porous volcanic rocks (see Heap and Violay (2021)
544 for a review). The pore-crack model describes a two-dimensional elastic medium populated
545 with circular pores of a uniform radius. In the model, cracks can propagate in a direction
546 parallel to the maximum principal stress when the stress at the tip of a crack on the curved
547 surface of the pore reaches the fracture toughness of the material, K_{IC} (the resistance of a
548 brittle material to the propagation of cracks under an applied stress). Eventually, the cracks
549 grow long enough to interact and ultimately coalesce, resulting in the macroscopic failure of
550 the medium. Although the andesites studied here contain microcracks, their microstructure
551 can be well approximated by this inclusion model (i.e. pores within a groundmass; Heap et al.,
552 2021a), although we highlight that the model assumes a uniform pore radius. In the analytical
553 solution to the model (Equation (1)), uniaxial compressive strength (UCS) is a function of K_{IC}
554 , porosity, ϕ, and pore radius, r. The two unknowns in Equation (1) are K_{IC} and r. We can
555 estimate r using microstructural analysis. To do so, we calculated the average equivalent
556 macropore diameter (excluding pores with a diameter < 30 μm) of each block using scanning
557 electron microscope images and open-source image analysis software ImageJ (data available
558 in Table 4). The average equivalent macropore diameter, $2r$, was calculated using
559 $2r = 3/2(d_F)$, where d_F is the average macropore Feret diameter. An example of how the
560 average equivalent macropore diameter was determined is available as Supplementary

561 Information. Values of dry and wet K_{IC} were then estimated using Equation (1), taking the
562 average values of dry and wet UCS for each block (Table 2). Dry and wet K_{IC}, and the wet to
563 dry K_{IC} ratio, are plotted as a function of alteration in Figures 9a and 9b, respectively (data
564 available in Table 4). The data of Figure 9 highlight that (1) wet K_{IC} is lower than dry K_{IC}
565 and (2) the reduction in K_{IC} in the presence of water is increased as a function of increasing
566 alteration. Using this approach, the wet to dry K_{IC} ratio for the andesites studied herein is
567 estimated to be between 0.32 and 0.93 (Figure 9). For the most part, these values are lower
568 than those typically reported in published studies. For example, ratios for a suite of sandstones
569 were measured to be between 0.65 and 0.95 (Noël et al., 2021), and the ratio for an unaltered
570 andesite (Kumamoto andesite) was measured to be 0.87 (Nara et al., 2012). We emphasise
571 that the values of K_{IC} provided in Figure 9 and Table 4 are estimates made using the pore-
572 emanating crack model (Equation (1)), and not measured values of K_{IC} as in Noël et al.
573 (2021) and Nara et al. (2012).

574 A reduction in the K_{IC} of rocks in the presence of water has been observed by many
575 experimental studies and has been attributed to several, potentially coeval, factors: a reduction
576 in surface energy due to water adsorption (Baud et al., 2000; Noël et al., 2021), crack-tip
577 capillary forces (Nara et al., 2012), grain-contact lubrication (Guha Roy et al., 2017), stress
578 corrosion cracking (Kataoka et al., 2015), mineral dissolution (Maruvanchery and Kim,
579 2019), and the presence of clay minerals (Wang et al., 2007; Nara et al., 2012). The reduction
580 in K_{IC} in the presence of water observed here (Figure 9a), is likely due to a combination of
581 these mechanisms; although, given that we provide here the short-term mechanical strength
582 (UCS experiments performed at a strain rate of 10^{-5} s^{-1}), we anticipate only minor
583 contributions from stress corrosion cracking and mineral dissolution. We consider that the
584 increase in the reduction in K_{IC} in the presence of water as alteration increases (Figure 9b) is
585 most likely explained by the increasing abundance of hydrophilic minerals, such as alunite

586 and clay minerals, as a function of increasing alteration (Table 1). Hydrophilic minerals
587 expand upon saturation with water, resulting in a reduction in their mechanical resistance
588 (Nara et al., 2012). We further note that, if hydrophilic minerals expand upon saturation and
589 reduce ϕ and/or r, then the K_{IC} estimated for the altered rocks using Equation (1) would be
590 even lower than our estimations presented in Table 4 and Figure 9.

591 We conclude, therefore, that the water-weakening in the dome rocks measured herein
592 (i.e. the reduction in UCS; Figures 4, 5, 6, and 8) is likely due to a reduction in K_{IC} in the
593 presence of water (Figure 9a). The increase in water-weakening as a function of alteration
594 (Figure 5b) can be explained by the decrease in the wet to dry K_{IC} ratio as the degree of
595 alteration (i.e. the abundance of hydrophilic minerals) increases (Figure 9b). The higher the
596 wt% of secondary minerals such as alunite and clay minerals, the more K_{IC} is reduced when
597 the rock is wet, and the greater the macroscopic water-weakening.

598

Sample	**Weight percentage of secondary minerals**	**Average equivalent macropore diameter, r (μm)**	**Dry K_{IC} (MPa·m$^{-1/2}$)**	**Wet K_{IC} (MPa·m$^{-1/2}$)**	**Wet/dry K_{IC} ratio**
H2A	23	179	0.43	0.35	0.82
H2B	75	173	0.06	0.02	0.31
H3	35	174	0.39	0.26	0.68
H4A	60	153	0.26	0.15	0.57
H5A	42	161	0.45	0.32	0.71
H6	53	145	0.34	0.24	0.70
H14	24	156	0.26	0.16	0.62
H15	61	180	0.19	0.11	0.60
H18	15	137	0.47	0.38	0.81
H20	45	167	0.04	0.03	0.74
H21	41	157	0.45	0.32	0.71
H22	17	88	0.53	0.46	0.88
H25	46	182	0.52	0.31	0.60
H29	16	204	0.43	0.35	0.81
H32	6	101	0.73	0.46	0.63
WP1285	13	69	0.26	0.21	0.79
WP1317	16	84	0.35	0.32	0.93

599

600 **Table 4**. Percentage of secondary minerals (i.e. alteration), average equivalent macropore
601 diameter, wet fracture toughness (K_{IC}), dry K_{IC}, and the wet to dry K_{IC} ratio for the samples
602 prepared for this study. Sample locations are provided in Figure 1b. Values of K_{IC} are
603 estimated using the analytical approximation of Sammis and Ashby's (1986) pore-emanating
604 crack micromechanical model provided by Zhu et al. (2010) (Equation (1)). The relative
605 uncertainties in the quantification of the mineral contents (Table 1) are on the order of 5–10%.
606

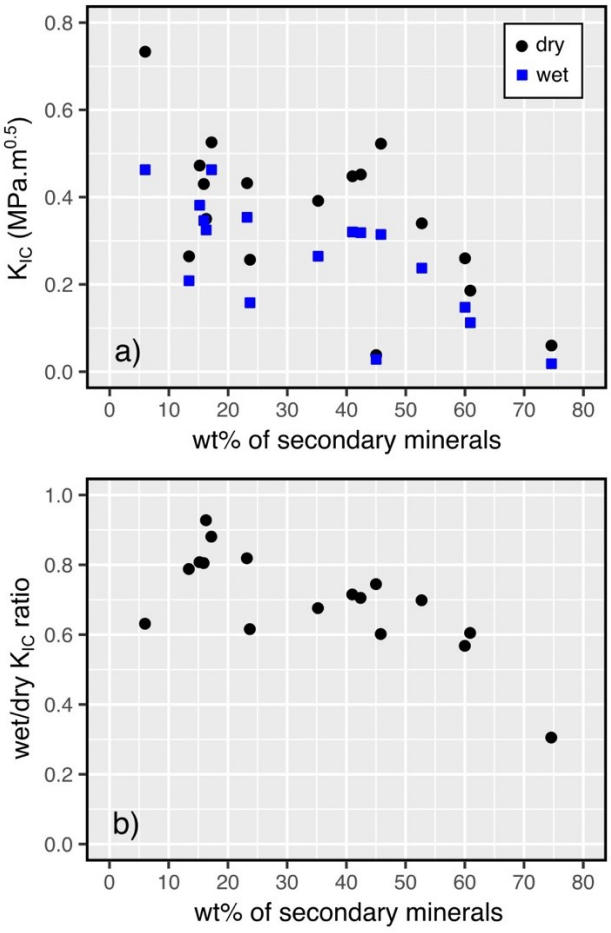

607

608 **Figure 9.** (a) Fracture toughness (K_{IC}) and (b) the wet to dry K_{IC} ratio as a function of the wt
609 % of secondary minerals (i.e. alteration) for samples from La Soufrière de Guadeloupe
610 (Eastern Caribbean). Values of K_{IC} are estimated using the analytical approximation of
611 Sammis and Ashby's (1986) pore-emanating crack micromechanical model provided by Zhu

et al. (2010) (Equation (1)). The relative uncertainties in the quantification of the mineral contents (Table 1) are on the order of 5–10%.

We highlight that we have performed experiments on completely dry and completely water-saturated samples. However, in nature, the rocks forming a volcanic edifice or dome likely exist between these two end-members (i.e. partially-saturated). Previous experimental work has shown that the water-weakening observed at 100% saturation in sandstones can be observed at saturation levels as low as 10%, whereas the compressive strength of shale decreased almost linearly as a function of increasing saturation level (Schmitt et al., 1994). Systematic uniaxial compressive strength measurements on partially-saturated volcanic rocks, which preserve different porosities and alteration intensities, are now required to understand whether the water-weakening observed here at 100% saturation (Figure 5) is also observed at lower levels of saturation. Finally, we note that we have used deaired, deionised water for our experiments. However, hydrothermal fluids, for example, are often characterised by low values of pH (e.g., Delmelle et al., 2000) which can influence the short-term strength of rock (e.g., Singh et al., 1999). Future experimental studies should also explore the influence of fluid composition and pH on the short-term strength of variably porous and variably altered volcanic rock.

5.3 The influence of water-saturation on dome stability

We performed numerical simulations in PFC to better understand the influence of water-saturation on dome stability. As explained in our methods section above, we first prepared initially stable dry unaltered and altered domes, guided by our experimental data (Table 2). For the dry unaltered dome, we determined the contact bond parameters required to give uniaxial compressive strength, tensile strength, and Young's modulus values of 100 MPa,

637 10 MPa, and 25 GPa, respectively (Figure 10a). These values were chosen to represent the
638 samples in our dataset that are characterised by low levels of alteration (e.g., samples H18,
639 H22, WP1317). For the dry altered dome, we determined the contact bond parameters
640 required to give uniaxial compressive strength, tensile strength, and Young's modulus values
641 of 10 MPa, 1 MPa, and 2 GPa, respectively (Figure 10c). These values were chosen to
642 represent the samples in our dataset that are characterised by high levels of alteration (e.g.,
643 sample H2B). We used a bulk density of 2400 and 1500 kg/m^3 for unaltered and altered dry
644 rocks, respectively, as guided by our experimental data. To investigate the influence of water-
645 saturation at the dome scale, we then changed all of the contact bond parameters in the model
646 to those representative of wet rocks (i.e. a completely water-saturated dome). Guided by our
647 experimental data (Figures 5b and 5d), we assumed wet to dry uniaxial compressive strength
648 and Young's modulus ratios for unaltered and altered dome rocks of 0.9 and 0.4, respectively.
649 Therefore, we determined the contact bond parameters required to give uniaxial compressive
650 strength, tensile strength, and Young's modulus of 90 MPa, 9 MPa, and 20 GPa, respectively,
651 for the unaltered dome (Figure 10b) and, for the altered dome, we used values of 4 MPa, 0.4
652 MPa, and 1 GPa, respectively (Figure 10d). We also note that, similar to the experimental data
653 shown in Figure 3, the strain required for failure in the model is also reduced upon saturation
654 with water. Guided by our experimental data, we used a bulk density of 2550 and 1900 kg/m^3
655 for unaltered and altered wet rocks, respectively. Finally, we highlight that, although
656 alteration is thought to have reduced the strength of the dome rocks from La Soufrière de
657 Guadeloupe (Figure 4b; see also discussions in Heap et al., 2021a, 2022a), alteration has also
658 been observed, or inferred, to increase the strength of volcanic rocks (e.g., Frolova et al.,
659 2014; Pola et al., 2014; Wyering et al., 2014; Coats et al., 2018; Heap et al., 2020b, 2021b;
660 Kanakiya et al., 2021, 2022). Although the rocks in these studies contain minerals such as
661 kaolinite and alunite, minerals that may promote water-weakening, it is unclear at present

whether volcanic rocks that exhibit a strengthening resulting from alteration would be, as seen for the rocks from La Soufrière de Guadeloupe (Figures 4, 5, 6, and 8), weaker in the presence of water. As a result, until new experimental data are available, the numerical modelling presented herein should be considered applicable for scenarios in which alteration reduces strength.

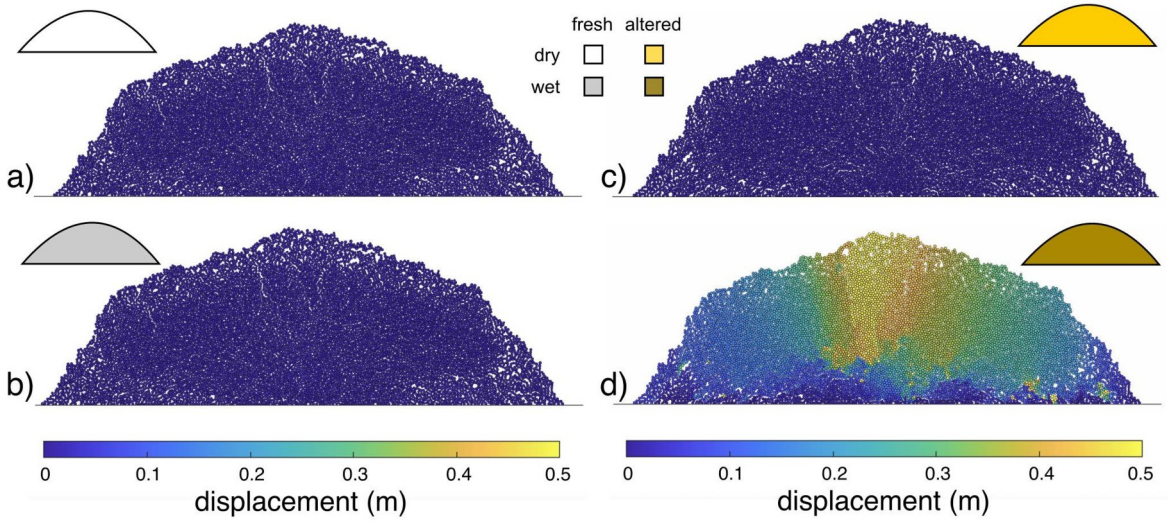

Figure 9. A stable (i.e. no displacement) dome generated in Particle Flow Code (PFC) for a (a) dry unaltered dome and (c) dry altered dome. (b) The displacement in the dome shown in (a) resulting from changing the mechanical properties of the contacts in the stable dome to represent wet unaltered rock. (d) The displacement in the dome shown in (c) resulting from changing the mechanical properties of the contacts to represent wet altered rock. Blue - low displacement; yellow - high displacement.

The results of the modelling show that displacements across the unaltered dome are essentially zero when the dome is water-saturated (Figure 10b), suggesting that water-saturation alone does not significantly influence the stability of an unaltered dome. By contrast, displacements are high (up to 0.5 m) when the altered dome is water-saturated, with the highest displacements concentrated at the centre of the dome (Figure 10d). Therefore, if

681 an altered dome becomes saturated by, for example, heavy rainfall or rising hydrothermal
682 fluids, the stability of the dome could be compromised, potentially promoting mass-wasting
683 events (e.g., partial dome collapse). We highlight that the propensity for such an altered water
684 saturated dome to collapse will likely be significantly enhanced if the dome is resting on a
685 sloping substratum (see, for example, Harnett and Heap, 2021) or comprises listric low-
686 strength layers from previous partial flank collapses that are opened in the direction of
687 maximum slope.

688 The scenarios shown in Figure 10 represent end-member scenarios in which the dome
689 is either completely unaltered or completely altered. In nature, hydrothermal alteration is
690 likely to be heterogeneously distributed within a dome (e.g., along permeable discontinuities).
691 Therefore, we performed additional modelling in which we included a buried altered zone
692 within an otherwise unaltered dome (Figure 11). In the first scenario, both the unaltered and
693 altered regions were dry (Figure 11b). In this scenario, only minor displacement is observed
694 within and above the buried altered zone (Figure 11b). In the second scenario, both the
695 unaltered and altered regions were water-saturated (Figure 11c). In this scenario, larger
696 displacements are observed within the altered zone, and notable displacements are also
697 observed on the half of the dome containing the buried alteration zone (Figure 11c). In other
698 words, dome instability was exacerbated following saturation in the presence of
699 hydrothermally altered materials. Therefore, the stability of a dome can be compromised by
700 water-saturation (e.g., heavy rainfall, changes to the hydrothermal system, and/or influx of
701 seawater) even when only a small portion of the dome is hydrothermally altered. It is likely,
702 in this scenario, that dome stability would be compromised more by alteration zones at or near
703 the base of the dome, rather than at the top of the dome.

704 The results of our modelling (Figures 10 and 11) may help explain why the frequency
705 of landslides and the failure and collapse of volcanic slopes and domes increases following

heavy rainfall (Kerle and van Wyk de Vries, 2001; Matthews et al., 2002; Matthews and Barclay, 2004; Elsworth et al., 2004; Simmons et al., 2004; Taron et al., 2007; Saucedo et al., 2008; Hicks et al., 2010; Vázquez et al., 2022).

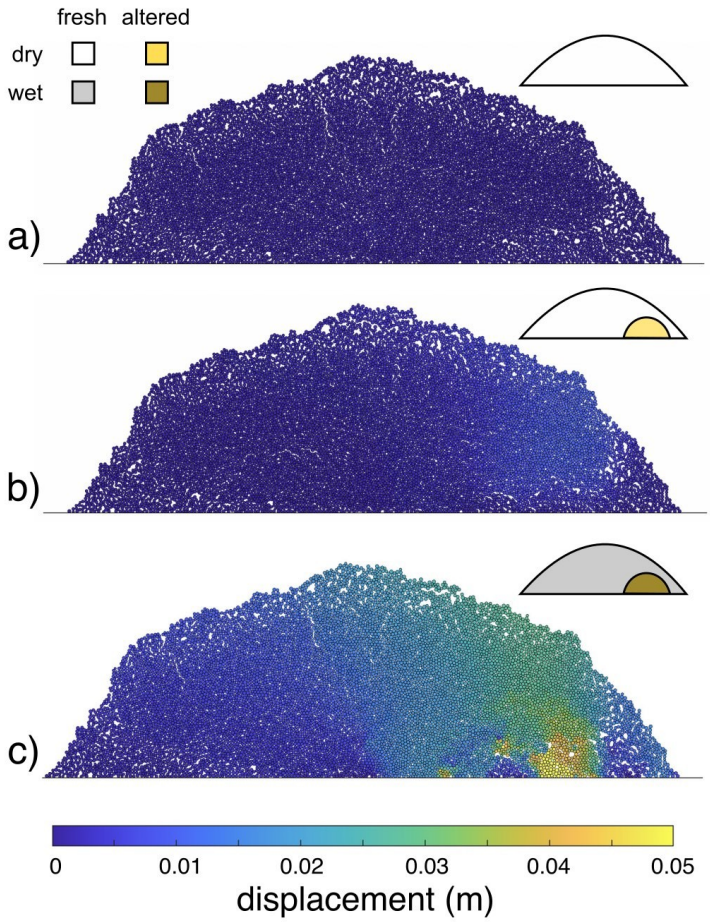

Figure 11. (a) Stable (i.e. no displacement) dry altered dome generated in Particle Flow Code (PFC). (b) The displacement in the dome shown in (a) resulting from adding a buried dry alteration zone within a dry unaltered dome (as in Harnett et al., 2022). (c) The displacement in the dome shown in (a) resulting from adding a buried wet alteration zone within a wet unaltered dome. Blue - low displacement; yellow - high displacement.

Extreme or heavy rainfall has been linked to multiple volcanic hazards (McKee et al., 1981; Matthews et al., 2002; Barclay et al., 2006), with theorised mechanisms that range from

719 deep-seated saturation and stress perturbations (McBirney, 1955; Violette et al., 2001;
720 Farquharson and Amelung, 2020; Sahoo et al., 2022) to shallow-seated processes operating in
721 the dome or upper edifice. Of these, the latter is often explained in terms of volumetric
722 expansion of liquids as a function of fuel-coolant interactions (Elsworth et al., 2004; Simmons
723 et al., 2004; Taron et al., 2007), with dome pressurisation and/or weakening driven by thermal
724 stress mechanisms (i.e. contraction of the dome carapace; Mastin, 1994; Yamasato et al.,
725 1998; Elsworth et al., 2004), or the stress on surrounding host-rock caused by the rapid
726 growth of a dome or cryptodome at shallow depth (Voight et al., 1981, 2002; Young et al.,
727 2002). More broadly, the saturation state of the edifice is thought to play an important role in
728 volcano destabilisation (McGuire, 1996; Day, 1996; Delcamp et al., 2016; Ball et al., 2018;
729 Finn et al., 2018; Heap et al., 2021b) and other failure processes, such as the failure of magma
730 reservoirs (Albino et al., 2018). Large-scale sector collapse events are also thought to be
731 facilitated by precipitation-induced retrogressive headward erosion and the weakening of
732 former partial flank collapse slip surfaces following precipitation (Kerle and van Wyk de
733 Vries, 2001; Kerle et al., 2003; Capra, 2006; Tost and Cronin, 2016; Romero et al., 2021).
734 Our new data presented here points to an additional role of dome or edifice rock saturation in
735 promoting volcano instability, in that saturation with water results in a reduction of rock
736 strength of ~10–60% (Figure 5a).

737 The distribution and degree of hydrothermal alteration throughout a volcanic edifice is
738 also thought to be key in determining the potential for collapse-related hazards. Commonly
739 occurring hydrothermal mineral assemblages are thought to have a deleterious effect on
740 volcano stability (López and Williams, 1993; Watters et al., 2000; van Wyk de Vries et al.,
741 2000; Reid et al., 2001; Voight et al., 2002; Reid, 2004; Cecchi et al., 2004; Salaün et al.,
742 2011; Ball et al., 2015; Detienne et al., 2017; Norini et al., 2020; Heap et al., 2021a), as
743 supported by geomechanical studies on the role of hydrothermal alteration in reducing the

744 strength of volcanic materials (in both natural and laboratory settings; Moon and
745 Jayawardane, 2004; de Potro and Hürlimann, 2009; Pola et al., 2014; Wyering et al., 2014;
746 Farquharson et al., 2019; Mordensky et al., 2019; Heap et al., 2021a, 2022a; Darmawan et al.,
747 2022). Indeed, structural failure is often spatially coincident with hydrothermal alteration
748 (Siebert et al., 1987; Delmelle et al., 2015); for example, Zimbelman (1996) notes the
749 association of alteration minerals—including alunite, jarosite, and other sulphates—with
750 exposed collapse scars, and Zimbelman et al. (2005) link collapse events at andesitic arc
751 volcanoes to veins of alteration minerals resulting from the mixing of magmagenic sulphate
752 and meteoric water. Indeed, Voight et al. (2002) found varicoloured hydrothermally altered
753 materials within avalanche deposits at Soufrière Hills volcano (Montserrat, Eastern
754 Caribbean). This link is congruent with observations at La Soufrière de Guadeloupe, where
755 avalanche deposits and material ejected during phreatic explosions were found to contain
756 various parts of the active and ancient hydrothermal systems of the volcano (as evidenced by
757 an acid-sulphate mineral assemblage; Salaün et al., 2011; Heap et al., 2021a), and collapse
758 events have revealed visibly altered material beneath (see Figure 1b). La Soufrière de
759 Guadeloupe is characterised by a vigorous hydrothermal system (Komorowski et al., 2005;
760 Villemant et al., 2005; Nicollin et al., 2006; Coutant et al., 2012; Lesparre et al., 2012;
761 Brothelande et al., 2014; Villemant et al., 2014; Rosas-Carbajal et al., 2016, 2017; Moretti et
762 al., 2020; Gibert et al., 2022) and, notably, weathering fluxes on the volcano are among the
763 highest recorded in tropical volcanic settings (Dessert et al., 2015). Our new data underscore
764 the importance of this hydrothermal alteration on the mechanical properties of dome-forming
765 rocks (Figure 5b), with UCS decreasing by as much as ~60% upon water-saturation for highly
766 altered materials (i.e. with a high proportion of secondary minerals). These data further
767 highlight how and why hydrothermal alteration and water (meteoric, hydrothermal, or
768 seawater) conspire to destabilise volcanic structures, as outlined in disastrous effect by the

1998 collapse at Casita volcano (van Wyk de Vries et al., 2000; Kerle and van Wyk de Vries, 2001; Kerle et al., 2003; Opfergelt et al., 2006) and several large rain-triggered collapses during the period of active dome growth at Soufrière Hills volcano (Elsworth et al., 2004; Simmons et al., 2004; Taron et al., 2007).

Based on observations of rainfall-induced dome instability at Soufrière Hills volcano, previous research has focussed on developing mechanistic models of dome collapse as a function of local rainfall rate (Elsworth et al., 2004; Matthews and Barclay, 2004; Taron et al., 2007; see also Harnett et al., 2019) thereby—directly or indirectly—accounting for the saturation state. In contrast, numerous studies that model the influence of alteration on dome or flank stability do not consider the presence or absence of interstitial fluids on the mechanical properties of the dome-forming materials. Critically, our modelling results (Figures 10 and 11) demonstrate that mechanical failure is promoted when both hydrothermal alteration and water-saturation operate in tandem. We emphasise that mechanical water-weakening is an important additional mechanism that has generally not been considered in existing stability modelling of domes, but that can facilitate collapse, particularly in the likely scenario when alteration is also present (Figures 10 and 11). We suggest that, when appropriate and where available, volcano stability models use data relevant for water-saturated volcanic rocks. We consider this especially relevant for submarine, coastal, and ocean-island volcanoes. For the modelling of coastal and ocean-island volcanoes, it is likely important to not only consider the partially saturated subaerial part of the volcano, but also the saturated submarine part (the importance of not neglecting the submarine portion of a coastal volcano is discussed in Urlaub et al., 2018).

We also highlight that the link between mechanical water-weakening and hydrothermal alteration may also be further exacerbated when hot gases and rising hydrothermal/magmatic fluids interact with water-saturated altered zones at shallow levels

794 within a dome or volcano, generating large volumes of steam and elevated fluid pore
795 pressures. Indeed, previous modelling has shown that elevated pore pressure negatively
796 impacts volcano stability (Reid, 2004; Heap et al., 2021b). The rise of large volumes of
797 hydrothermal fluids due to major heat pulses was observed during all phreatic unrest and
798 eruptions at La Soufrière of Guadeloupe (Komorowski et al., 2005; Rosas-Carbajal et al.,
799 2016) and Mount Pelée in 1902 (Tanguy, 1994), and is characteristic of the ongoing unrest at
800 La Soufrière of Guadeloupe (Moretti et al., 2020), underscoring the importance of
801 incorporating these phenomena into future, more complex volcano stability models.

802 By combining our experimental results with analytical and numerical mechanical
803 modelling, we link the micro-scale effects of hydrothermal alteration on the fracture
804 mechanics to the scale of the dome. These considerations are particularly important in light of
805 projected climate futures (Aubry et al., 2022). As circulation models results in Figure 1c
806 highlight, La Soufrière de Guadeloupe is projected to receive increasing amounts of heavy
807 rainfall over the next 80 years (see also Cantet et al., 2014), even given widespread adoption
808 of stringent climate change mitigation policies. Accordingly, the propensity for rainfall-
809 induced collapse events will likely increase as well, and detecting where potential collapse
810 events may occur becomes ever more crucial, especially given the absence of detectable
811 geophysical signals preceding such events (Matthews et al., 2002). Our model results
812 highlight that identifying zones of (potentially concealed) hydrothermal alteration may prove
813 to be key in mitigating such hazards (Darmawan et al., 2022; Harnett et al., 2022). Moreover,
814 our results emphasise that close monitoring of domes and slopes during and following heavy
815 rainfall is essential: we echo the call of Barclay et al. (2006) for routine incorporation of
816 meteorological data into monitoring praxis. Finally, direct knowledge of the state of edifice or
817 dome saturation could be invaluable for future stability monitoring. Our new data and models
818 add a new importance to the 3D characterisation of water saturation in volcanic edifices, as

well as its evolution over time, using geophysical methods. For example, geophysical methods such as electrical resistivity tomography (e.g. Rosas-Carbajal et al., 2016) and muon tomography (Rosas-Carbajal et al., 2017; Bajou et al., 2023) are sensitive to water content and could be repeatedly employed to assess the distribution of water in the upper parts of the volcanic edifice. Both seismic noise interferometry (Sens-Schönfelder and Wegler, 2006), a method increasingly used to monitor water level variations, and the satellite-based monitoring of groundwater (Rodell et al., 2009) could also be powerful tools to track edifice or dome saturation. Finally, borehole dilatometers and piezometers (Hurwitz and Johnston, 2003) could provide punctual and precise data to calibrate numerical models and interpret geophysical imaging.

While La Soufrière de Guadeloupe has been chosen as a case study herein, for the reasons outlined in section two, we emphasise that our conclusions are much more broadly applicable. Volcanoes exhibiting zones of intense alteration and/or vigorous hydrothermal systems (Africano and Bernard, 2000; Zimbelman et al., 2005; Rodríguez and van Bergen, 2017; Yilmaz et al., 2021), as well as those with persistent acid lakes (van Hinsberg et al., 2010; Rouwet et al., 2014; Delmelle et al., 2015), will likely be particularly prone to extensive water-weakening, and therefore heightened instability, in the event of edifice and/or dome saturation. In tropical environments, increasingly frequent bouts of intense precipitation (not only during the so-called hurricane or rainy season but also at other times of the year in the Tropics) may directly trigger mass-wasting events (as observed elsewhere in the Caribbean: Matthews et al., 2002; Carn et al., 2004; Taron et al., 2007; Matthews et al., 2009 and in other settings: Yamasato et al., 1998; Elsworth et al., 2004), or facilitate other internal or external trigger mechanisms such as magma movement (Reid et al., 2010), pressurisation (Reid, 2004; Heap et al., 2021b), or basal spreading (van Wyk de Vries and Francis, 1997). For the majority of subaerial volcanoes, climate models project an increase in such meteorological

844 events (Farquharson and Amelung, 2022). In the context of water-weakening and related
845 hazards, climate change may also be important in terms of sea level rise. Analysis of drill
846 cores from offshore Montserrat shows that Soufrière Hills volcano underwent periods of
847 heightened instability during periods of rapid sea level rise, with all three large collapse
848 events at the volcano being correlated with sea level changes of > 5 m/ka (Coussens et al.,
849 2016); those authors also highlight that this phenomenon appears to echo a broader trend
850 across other island arc volcanoes. We further posit that variation in edifice saturation due to
851 sea level rise could also promote instability in coastal or island arc volcanoes.
852
853 **6 Conclusions**
854 The goal of this study, using dome stability models informed by experimental data,
855 was to investigate whether water-saturation alone can jeopardise the stability of a lava dome.
856 Our experiments show that water-saturation reduced the strength of variably-altered dome
857 rocks, and that water-weakening increased as the degree of alteration increased.
858 Micromechanical modelling suggested that the observed water-weakening was the result of a
859 decrease in fracture toughness, K_{IC}, in the presence of water. The ratio of wet to dry K_{IC} also
860 decreased with increasing alteration, explaining the trend of increasing water-weakening with
861 increasing alteration. Dome stability modelling, informed by our experimental data, showed
862 that the stability of a lava dome can be compromised by water-saturation if the dome is
863 altered, or contains an altered zone (even without the compounding exacerbating effects of
864 volcanic unrest, such as seismicity, deformation, high heat fluxes, and rising fluids). The
865 models presented herein may therefore help explain why the frequency of landslides and the
866 failure and collapse of altered volcanic slopes and dome increases following heavy rainfall.
867 Our study highlights, and especially in the light of predicted increases in heavy rainfall due to
868 climate change, that the degree of alteration and water-saturation should be monitored at

active volcanoes worldwide, volcanic domes and slopes should be closely monitored following heavy rainfall, and that large-scale volcano stability models should use values for water-saturated rocks where and when appropriate.

Acknowledgements

This work was supported by ANR grant MYGALE ("Modelling the phYsical and chemical Gradients of hydrothermal ALteration for warning systems of flank collapse at Explosive volcanoes"; ANR-21-CE49-0010). M. Heap also acknowledges support from the Institut Universitaire de France (IUF). We thank Tomaso Esposti Ongaro and Lucille Carbillet for help in the field, Laurent Gastaldo and Bertrand Renaudie for help in the laboratory, and all those working at the Observatoire Volcanologique et Sismologique de Guadeloupe (OVSG). This research was also supported by two Hubert Curien Partnership (PHC) grants: a Germaine de Staël grant awarded to M. Heap and M. Violay (grant number 47712SB) and a Ulysses grant awarded to M. Heap and C. Harnett (grant number 47199ZM). The Germaine de Staël grant is implemented by the Ministry for Higher Education, Research, and Innovation (MESRI) and the Ministry for Europe and Foreign Affairs (MEAE) in France, and by the State Secretariat for Education, Research, and Innovation (SERI) and the Swiss Academy of Technical Sciences (SATW) in Switzerland. The Ulysses grant is implemented by the MEAE and the MESRI in France, and by the Irish Research Council (IRC) in Ireland. This research also benefitted from European Research Council Starting Grant BEFINE (ERC-2017-STG), awarded to M. Violay. We thank the IPGP for general funding for the Observatoires Volcanologiques et Sismologiques (OVS), INSU-CNRS for the funding provided to the Service National d'Observation en Volcanologie (SNOV), and the Ministère pour la Transition Ecologique (MTE) for financial support for the monitoring of the unstable flank of La Soufrière de Guadeloupe. We are grateful to the Parc National de la Guadeloupe for

allowing us to carry out geological fieldwork on La Soufrière de Guadeloupe. Finally, we thank The Fleet (Dublin, Ireland) for their hospitality. The constructive comments of Shane Cronin, Ludmila Adam, and Anthony Lamur helped improve this manuscript.

References

Africano, F., & Bernard, A. (2000). Acid alteration in the fumarolic environment of Usu volcano, Hokkaido, Japan. Journal of Volcanology and Geothermal Research, 97(1-4), 475-495.

Aizawa, K., Ogawa, Y., & Ishido, T. (2009). Groundwater flow and hydrothermal systems within volcanic edifices: Delineation by electric self-potential and magnetotellurics. Journal of Geophysical Research: Solid Earth, 114(B1).

Albino, F., Amelung, F., & Gregg, P. (2018). The role of pore fluid pressure on the failure of magma reservoirs: insights from Indonesian and Aleutian arc volcanoes. Journal of Geophysical Research: Solid Earth, 123(2), 1328-1349.

Allemand, P., Delacourt, C., Lajeunesse, E., Devauchelle, O., & Beauducel, F. (2014). Erosive effects of the storm Helena (1963) on Basse Terre Island (Guadeloupe—Lesser Antilles Arc). Geomorphology, 206, 79-86.

Apuani, T., Corazzato, C., Cancelli, A., & Tibaldi, A. (2005). Stability of a collapsing volcano (Stromboli, Italy): Limit equilibrium analysis and numerical modelling. Journal of Volcanology and Geothermal Research, 144(1-4), 191-210.

Atkinson, B. K. (1984). Subcritical crack growth in geological materials. Journal of Geophysical Research: Solid Earth, 89(B6), 4077-4114.

Aubry, T. J., Farquharson, J. I., Rowell, C. R., Watt, S. F., Pinel, V., Beckett, F., ... & Sykes, J. S. (2022). Impact of climate change on volcanic processes: current understanding and future challenges. Bulletin of Volcanology, 84(6), 58.

Bajou, R., Rosas-Carbajal, M., Tonazzo, A., & Marteau, J. (2023). High-resolution structural imaging of volcanoes using improved muon tracking. Geophysical Journal International, 235(2), 1138-1149.

Ball, J. L., Stauffer, P. H., Calder, E. S., & Valentine, G. A. (2015). The hydrothermal alteration of cooling lava domes. Bulletin of Volcanology, 77, 1-16.

Ball, J. L., Taron, J., Reid, M. E., Hurwitz, S., Finn, C., & Bedrosian, P. (2018). Combining multiphase groundwater flow and slope stability models to assess stratovolcano flank collapse in the Cascade Range. Journal of Geophysical Research: Solid Earth, 123(4), 2787-2805.

Barclay, J., Johnstone, J. E., & Matthews, A. J. (2006). Meteorological monitoring of an active volcano: implications for eruption prediction. Journal of volcanology and geothermal research, 150(4), 339-358.

Baud, P., Zhu, W., & Wong, T. F. (2000). Failure mode and weakening effect of water on sandstone. Journal of Geophysical Research: Solid Earth, 105(B7), 16371-16389.

Baud, P., Reuschlé, T., Ji, Y., Cheung, C. S., & Wong, T. F. (2015). Mechanical compaction and strain localization in Bleurswiller sandstone. Journal of Geophysical Research: Solid Earth, 120(9), 6501-6522.

Baud, P., Rolland, A., Heap, M., Xu, T., Nicolé, M., Ferrand, T., ... & Conil, N. (2016). Impact of stylolites on the mechanical strength of limestone. Tectonophysics, 690, 4-20.

Borselli, L., Capra, L., Sarocchi, D., & De la Cruz-Reyna, S. (2011). Flank collapse scenarios at Volcán de Colima, Mexico: a relative instability analysis. Journal of Volcanology and Geothermal Research, 208(1-2), 51-65.

Boudon, G., Komorowski, J. C., Villemant, B., & Semet, M. P. (2008). A new scenario for the last magmatic eruption of La Soufrière of Guadeloupe (Lesser Antilles) in 1530 AD Evidence from stratigraphy radiocarbon dating and magmatic evolution of erupted products. Journal of Volcanology and Geothermal Research, 178(3), 474-490.

Brantut, N., Heap, M. J., Meredith, P. G., & Baud, P. (2013). Time-dependent cracking and brittle creep in crustal rocks: A review. Journal of Structural Geology, 52, 17-43.

Brombach, T., Marini, L., & Hunziker, J. C. (2000). Geochemistry of the thermal springs and fumaroles of Basse-Terre Island, Guadeloupe, Lesser Antilles. Bulletin of Volcanology, 61, 477-490.

Brothelande, E., Finizola, A., Peltier, A., Delcher, E., Komorowski, J. C., Di Gangi, F., ... & Legendre, Y. (2014). Fluid circulation pattern inside La Soufrière volcano (Guadeloupe) inferred from combined

electrical resistivity tomography, self-potential, soil temperature and diffuse degassing measurements. Journal of Volcanology and Geothermal Research, 288, 105-122.
de Bremond d'Ars, J., & Gibert, D. (2022). Multiscale external rainfall forcing from high-resolution temperature time series of fumaroles at La Soufrière de Guadeloupe volcano. Frontiers in Earth Science, 9, 1364.
del Potro, R., & Hürlimann, M. (2009). The decrease in the shear strength of volcanic materials with argillic hydrothermal alteration, insights from the summit region of Teide stratovolcano, Tenerife. Engineering Geology, 104(1-2), 135-143.
Cantet, P., Déqué, M., Palany, P., & Maridet, J. L. (2014). The importance of using a high-resolution model to study the climate change on small islands: the Lesser Antilles case. Tellus A: Dynamic Meteorology and Oceanography, 66(1), 24065.
Capra, L. (2006). Abrupt climatic changes as triggering mechanisms of massive volcanic collapses. Journal of Volcanology and Geothermal Research, 155(3-4), 329-333.
Carn, S. A., Watts, R. B., Thompson, G., & Norton, G. E. (2004). Anatomy of a lava dome collapse: the 20 March 2000 event at Soufrière Hills Volcano, Montserrat. Journal of Volcanology and Geothermal Research, 131(3-4), 241-264.
Carr, B. B., Lev, E., Vanderkluysen, L., Moyer, D., Marliyani, G. I., & Clarke, A. B. (2022). The stability and collapse of lava domes: Insight from photogrammetry and slope stability models applied to Sinabung volcano (Indonesia). Frontiers in Earth Science, 10, 813813.
Caselle, C., Baud, P., Kushnir, A. R. L., Reuschlé, T., & Bonetto, S. M. R. (2022). Influence of water on deformation and failure of gypsum rock. Journal of Structural Geology, 163, 104722.
Castagna, A., Ougier-Simonin, A., Benson, P. M., Browning, J., Walker, R. J., Fazio, M., & Vinciguerra, S. (2018). Thermal damage and pore pressure effects of the Brittle-Ductile transition in comiso limestone. Journal of Geophysical Research: Solid Earth, 123(9), 7644-7660.
Cecchi, E., van Wyk de Vries, B., & Lavest, J. M. (2004). Flank spreading and collapse of weak-cored volcanoes. Bulletin of Volcanology, 67, 72-91.
Chester, F. M., & Logan, J. M. (1986). Implications for mechanical properties of brittle faults from observations of the Punchbowl fault zone, California. Pure and Applied Geophysics, 124, 79-106.
Coats, R., Kendrick, J. E., Wallace, P. A., Miwa, T., Hornby, A. J., Ashworth, J. D., ... & Lavallée, Y. (2018). Failure criteria for porous dome rocks and lavas: a study of Mt. Unzen, Japan. Solid Earth, 9, 1299-1328.
Coussens, M., Wall-Palmer, D., Talling, P. J., Watt, S. F., Cassidy, M., Jutzeler, M., ... & Stinton, A. J. (2016). The relationship between eruptive activity, flank collapse, and sea level at volcanic islands: A long-term (> 1 Ma) record offshore Montserrat, Lesser Antilles. Geochemistry, Geophysics, Geosystems, 17(7), 2591-2611.
Coutant, O., Bernard, M. L., Beauducel, F., Nicollin, F., Bouin, M. P., & Roussel, S. (2012). Joint inversion of P-wave velocity and density, application to La Soufrière of Guadeloupe hydrothermal system. Geophysical Journal International, 191(2), 723-742.
Darmawan, H., Troll, V. R., Walter, T. R., Deegan, F. M., Geiger, H., Heap, M. J., ... & Müller, D. (2022). Hidden mechanical weaknesses within lava domes provided by buried high-porosity hydrothermal alteration zones. Scientific Reports, 12(1), 3202.
Day, S. J. (1996). Hydrothermal pore fluid pressure and the stability of porous, permeable volcanoes. Geological Society, London, Special Publications, 110(1), 77-93.
Delcamp, A., Roberti, G., & van Wyk de Vries, B. (2016). Water in volcanoes: evolution, storage and rapid release during landslides. Bulletin of Volcanology, 78, 1-12.
Delmelle, P., Bernard, A., Kusakabe, M., Fischer, T. P., & Takano, B. (2000). Geochemistry of the magmatic–hydrothermal system of Kawah Ijen volcano, East Java, Indonesia. Journal of Volcanology and Geothermal research, 97(1-4), 31-53.
Delmelle, P., Henley, R. W., Opfergelt, S., & Detienne, M. (2015). Summit acid crater lakes and flank instability in composite volcanoes. Volcanic lakes, 289-305.
Dessert, C., Lajeunesse, E., Lloret, E., Clergue, C., Crispi, O., Gorge, C., & Quidelleur, X. (2015). Controls on chemical weathering on a mountainous volcanic tropical island: Guadeloupe (French West Indies). Geochimica et Cosmochimica Acta, 171, 216-237.
Detienne, M., Delmelle, P., Guevara, A., Samaniego, P., Opfergelt, S., & Mothes, P. A. (2017). Contrasting origin of two clay-rich debris flows at Cayambe Volcanic Complex, Ecuador. Bulletin of Volcanology, 79, 1-14.
Duda, M., & Renner, J. (2013). The weakening effect of water on the brittle failure strength of sandstone. Geophysical Journal International, 192(3), 1091-1108.
Elsworth, D., Voight, B., Thompson, G., & Young, S. R. (2004). Thermal-hydrologic mechanism for rainfall-triggered collapse of lava domes. Geology, 32(11), 969-972.

Farquharson, J. I., Wild, B., Kushnir, A. R., Heap, M. J., Baud, P., & Kennedy, B. (2019). Acid-induced dissolution of andesite: evolution of permeability and strength. Journal of Geophysical Research: Solid Earth, 124(1), 257-273.

Farquharson, J. I., & Amelung, F. (2020). Extreme rainfall triggered the 2018 rift eruption at Kīlauea Volcano. Nature, 580(7804), 491-495.

Farquharson, J. I., & Amelung, F. (2022). Volcanic hazard exacerbated by future global warming-driven increase in heavy rainfall. Royal Society Open Science, 9(7), 220275.

Finn, C. A., Deszcz-Pan, M., Ball, J. L., Bloss, B. J., & Minsley, B. J. (2018). Three-dimensional geophysical mapping of shallow water saturated altered rocks at Mount Baker, Washington: Implications for slope stability. Journal of Volcanology and Geothermal Research, 357, 261-275.

Frolova, J., Ladygin, V., Rychagov, S., & Zukhubaya, D. (2014). Effects of hydrothermal alterations on physical and mechanical properties of rocks in the Kuril–Kamchatka island arc. Engineering Geology, 183, 80-95.

Frolova, J. V., Chernov, M. S., Rychagov, S. N., Ladygin, V. M., Sokolov, V. N., & Kuznetsov, R. A. (2021). The influence of hydrothermal argillization on the physical and mechanical properties of tuffaceous rocks: a case study from the Upper Pauzhetsky thermal field, Kamchatka. Bulletin of Engineering Geology and the Environment, 80, 1635-1651.

Fulignati, P. (2020). Clay minerals in hydrothermal systems. Minerals, 10(10), 919.

Gibert, D., de Bremond d'Ars, J., Carlus, B., Deroussi, S., Ianigro, J. C., Jessop, D. E., ... & Rosas-Carbajal, M. (2022). Observation of the Dynamics of Hydrothermal Activity in La Soufrière of Guadeloupe Volcano with Joint Muography, Gravimetry, Electrical Resistivity Tomography, Seismic and Temperature Monitoring. Muography: Exploring Earth's Subsurface with Elementary Particles, 55-73.

Guha Roy, D., Singh, T. N., Kodikara, J., & Talukdar, M. (2017). Correlating the mechanical and physical properties with mode-I fracture toughness of rocks. Rock Mechanics and Rock Engineering, 50, 1941-1946.

Harnett, C. E., Thomas, M. E., Purvance, M. D., & Neuberg, J. (2018). Using a discrete element approach to model lava dome emplacement and collapse. Journal of Volcanology and Geothermal Research, 359, 68-77.

Harnett, C. E., Kendrick, J. E., Lamur, A., Thomas, M. E., Stinton, A., Wallace, P. A., ... & Lavallée, Y. (2019). Evolution of mechanical properties of lava dome rocks across the 1995–2010 eruption of soufrière hills volcano, Montserrat. Frontiers in Earth Science, 7, 7.

Harnett, C. E., & Heap, M. J. (2021). Mechanical and topographic factors influencing lava dome growth and collapse. Journal of Volcanology and Geothermal Research, 420, 107398.

Harnett, C. E., Heap, M. J., Troll, V. R., Deegan, F. M., & Walter, T. R. (2022). Large-scale lava dome fracturing as a result of concealed weakened zones. Geology, 50(12), 1346-1350.

Hawkins, A. B., & McConnell, B. J. (1992). Sensitivity of sandstone strength and deformability to changes in moisture content. Quarterly Journal of Engineering Geology, 25(2), 115-130.

Heap, M. J., Kennedy, B. M., Pernin, N., Jacquemard, L., Baud, P., Farquharson, J. I., ... & Dingwell, D. B. (2015). Mechanical behaviour and failure modes in the Whakaari (White Island volcano) hydrothermal system, New Zealand. Journal of Volcanology and Geothermal Research, 295, 26-42.

Heap, M. J., Farquharson, J. I., Kushnir, A. R., Lavallée, Y., Baud, P., Gilg, H. A., & Reuschlé, T. (2018). The influence of water on the strength of Neapolitan Yellow Tuff, the most widely used building stone in Naples (Italy). Bulletin of Volcanology, 80, 1-15.

Heap, M. J., Villeneuve, M., Kushnir, A. R., Farquharson, J. I., Baud, P., & Reuschlé, T. (2019). Rock mass strength and elastic modulus of the Buntsandstein: an important lithostratigraphic unit for geothermal exploitation in the Upper Rhine Graben. Geothermics, 77, 236-256.

Heap, M. J., Villeneuve, M., Albino, F., Farquharson, J. I., Brothelande, E., Amelung, F., ... & Baud, P. (2020a). Towards more realistic values of elastic moduli for volcano modelling. Journal of Volcanology and Geothermal Research, 390, 106684.

Heap, M. J., Gravley, D. M., Kennedy, B. M., Gilg, H. A., Bertolett, E., & Barker, S. L. (2020b). Quantifying the role of hydrothermal alteration in creating geothermal and epithermal mineral resources: The Ohakuri ignimbrite (Taupō Volcanic Zone, New Zealand). Journal of Volcanology and Geothermal Research, 390, 106703.

Heap, M. J., Baumann, T. S., Rosas-Carbajal, M., Komorowski, J. C., Gilg, H. A., Villeneuve, M., ... & Reuschlé, T. (2021a). Alteration-Induced Volcano Instability at La Soufrière de Guadeloupe (Eastern Caribbean). Journal of Geophysical Research: Solid Earth, 126(8), e2021JB022514.

Heap, M. J., Baumann, T., Gilg, H. A., Kolzenburg, S., Ryan, A. G., Villeneuve, M., ... & Clynne, M. A. (2021b). Hydrothermal alteration can result in pore pressurization and volcano instability. Geology, 49(11), 1348-1352.

Heap, M. J., & Violay, M. E. (2021). The mechanical behaviour and failure modes of volcanic rocks: a review. Bulletin of Volcanology, 83(5), 33.

Heap, M. J., Harnett, C. E., Wadsworth, F. B., Gilg, H. A., Carbillet, L., Rosas-Carbajal, M., ... & Moretti, R. (2022a). The tensile strength of hydrothermally altered volcanic rocks. Journal of Volcanology and Geothermal Research, 428, 107576.

Heap, M. J., Jessop, D. E., Wadsworth, F. B., Rosas-Carbajal, M., Komorowski, J. C., Gilg, H. A., ... & Moretti, R. (2022b). The thermal properties of hydrothermally altered andesites from La Soufrière de Guadeloupe (Eastern Caribbean). Journal of Volcanology and Geothermal Research, 421, 107444.

Heap, M. J., Troll, V. R., Harris, C., Gilg, H. A., Moretti, R., Rosas-Carbajal, M., ... & Baud, P. (2022c). Whole-rock oxygen isotope ratios as a proxy for the strength and stiffness of hydrothermally altered volcanic rocks. Bulletin of Volcanology, 84(8), 74.

Heap, M. J., Harnett, C. E., Nazarbayov, T., Heng, Z., Baud, P., Xu, T., ... & Komorowski, J. C. (2023a). The influence of heterogeneity on the strength of volcanic rocks and the stability of lava domes. Bulletin of Volcanology, 85(9), 49.

Heap, M. J., Wadsworth, F. B., & Jessop, D. E. (2023b). The thermal conductivity of unlithified granular volcanic materials: The influence of hydrothermal alteration and degree of water saturation. Journal of Volcanology and Geothermal Research, 107775.

Hicks, P. D., Matthews, A. J., & Cooker, M. J. (2010). Triggering of a volcanic dome collapse by rainwater infiltration. Journal of Geophysical Research: Solid Earth, 115(B9).

Hurwitz, S., Kipp, K. L., Ingebritsen, S. E., & Reid, M. E. (2003). Groundwater flow, heat transport, and water table position within volcanic edifices: Implications for volcanic processes in the Cascade Range. Journal of Geophysical Research: Solid Earth, 108(B12).

Husain, T., Elsworth, D., Voight, B., Mattioli, G., & Jansma, P. (2014). Influence of extrusion rate and magma rheology on the growth of lava domes: Insights from particle-dynamics modeling. Journal of volcanology and geothermal research, 285, 100-117.

Husain, T., Elsworth, D., Voight, B., Mattioli, G., & Jansma, P. (2018). Influence of conduit flow mechanics on magma rheology and the growth style of lava domes. Geophysical Journal International, 213(3), 1768-1784.

Husain, T., Elsworth, D., Voight, B., Mattioli, G., & Jansma, P. (2019). Morphologic variation of an evolving dome controlled by the extrusion of finite yield strength magma. Journal of Volcanology and Geothermal Research, 370, 51-64.

Inoue, A. (1995). Formation of clay minerals in hydrothermal environments. Origin and Mineralogy of Clays: Clays and the Environment, 268-329.

Jessop, D. E., Moune, S., Moretti, R., Gibert, D., Komorowski, J. C., Robert, V., ... & Burtin, A. (2021). A multi-decadal view of the heat and mass budget of a volcano in unrest: La Soufrière de Guadeloupe (French West Indies). Bulletin of Volcanology, 83, 1-19.

Join, J. L., Folio, J. L., & Robineau, B. (2005). Aquifers and groundwater within active shield volcanoes. Evolution of conceptual models in the Piton de la Fournaise volcano. Journal of Volcanology and Geothermal Research, 147(1-2), 187-201.

Kanakiya, S., Adam, L., Rowe, M. C., Lindsay, J. M., & Esteban, L. (2021). The role of tuffs in sealing volcanic conduits. Geophysical Research Letters, 48(20), e2021GL095175.

Kanakiya, S., Adam, L., Rowe, M. C., Esteban, L., Lerner, G. A., & Lindsay, J. M. (2022). Petrophysical and elastic properties of altered lavas from Mt. Taranaki: Implications for dome stability. Journal of Volcanology and Geothermal Research, 432, 107693.

Kataoka, M., Obara, Y., & Kuruppu, M. (2015). Estimation of fracture toughness of anisotropic rocks by semi-circular bend (SCB) tests under water vapor pressure. Rock Mechanics and Rock Engineering, 48, 1353-1367.

Kendrick, J. E., Schaefer, L. N., Schauroth, J., Bell, A. F., Lamb, O. D., Lamur, A., ... & Kennedy, B. M. (2021). Physical and mechanical rock properties of a heterogeneous volcano: the case of Mount Unzen, Japan. Solid Earth, 12(3), 633-664.

Kerle, N., & De Vries, B. V. W. (2001). The 1998 debris avalanche at Casita volcano, Nicaragua—investigation of structural deformation as the cause of slope instability using remote sensing. Journal of Volcanology and Geothermal Research, 105(1-2), 49-63.

Kerle, N., van Wyk de Vries, B., & Oppenheimer, C. (2003). New insight into the factors leading to the 1998 flank collapse and lahar disaster at Casita volcano, Nicaragua. Bulletin of volcanology, 65, 331-345.

Komorowski, J.-C., Boudon, G., Semet, M., Beauducel, F., Anténor-Habazac, C., Bazin, S., & Hammmouya, G. (2005). Guadeloupe. In J. Lindsay, R. Robertson, J. Shepherd, & S. Ali (Eds.), Volcanic Atlas of the lesser Antilles (pp. 65– 102). University of the French West Indies, Seismic Research Unit.

Kranz, R. L., Harris, W. J., & Carter, N. L. (1982). Static fatigue of granite at 200 C. Geophysical Research Letters, 9(1), 1-4.

Le Friant, A., Boudon, G., Komorowski, J. C., Heinrich, P., & Semet, M. P. (2006). Potential flank-collapse of Soufriere Volcano, Guadeloupe, lesser Antilles? Numerical simulation and hazards. Natural hazards, 39, 381-393.

Legendre, Y. (2012). Reconstruction fine de l'histoire éruptive et scénarii éruptifs à la Soufrière de Guadeloupe : vers un modèle intégré de fonctionnement du volcan (Doctoral dissertation, Université Paris 7-Denis Diderot; Institut de Physique du Globe de Paris).

Lesparre, N., Gibert, D., Marteau, J., Komorowski, J. C., Nicollin, F., & Coutant, O. (2012). Density muon radiography of La Soufriere of Guadeloupe volcano: comparison with geological, electrical resistivity and gravity data. Geophysical Journal International, 190(2), 1008-1019.

Lesparre, N., Grychtol, B., Gibert, D., Komorowski, J. C., & Adler, A. (2014). Cross-section electrical resistance tomography of La Soufrière of Guadeloupe lava dome. Geophysical Journal International, 197(3), 1516-1526.

López, D. L., & Williams, S. N. (1993). Catastrophic volcanic collapse: relation to hydrothermal processes. Science, 260(5115), 1794-1796.

Maruvanchery, V., & Kim, E. (2019). Effects of water on rock fracture properties: Studies of mode I fracture toughness, crack propagation velocity, and consumed energy in calcite-cemented sandstone. Geomechanics and Engineering, 17(1), 57-67.

Mastin, L. G. (1994). Explosive tephra emissions at Mount St. Helens, 1989-1991: The violent escape of magmatic gas following storms? Geological Society of America Bulletin, 106(2), 175-185.

Masuda, K. (2001). Effects of water on rock strength in a brittle regime. Journal of Structural Geology, 23(11), 1653-1657.

Matthews, A. J., Barclay, J., Carn, S., Thompson, G., Alexander, J., Herd, R., & Williams, C. (2002). Rainfall-induced volcanic activity on Montserrat. Geophysical Research Letters, 29(13), 22-1.

Matthews, A. J., & Barclay, J. (2004). A thermodynamical model for rainfall-triggered volcanic dome collapse. Geophysical Research Letters, 31(5).

Matthews, A. J., Barclay, J., & Johnstone, J. E. (2009). The fast response of volcano-seismic activity to intense precipitation: triggering of primary volcanic activity by rainfall at Soufrière Hills Volcano, Montserrat. Journal of Volcanology and Geothermal Research, 184(3-4), 405-415.

McBirney, A. R. (1955). Thoughts on the eruption of the Nicaraguan Volcano Las Pilas. Bulletin Volcanologique, 17(1), 113-117.

McGuire, W. J. (1996). Volcano instability: a review of contemporary themes. Geological Society, London, Special Publications, 110(1), 1-23.

McKee, C. O., Wallace, D. A., Almond, R. A., & Talai, B. (1981). Fatal hydro-eruption of Karkar volcano in 1979: Development of a maar-like crater. In Cooke-Ravian Volume of Volcanological Papers (Vol. 10, pp. 63-84). Port Moresby, Papua New Guinea: Geological Survey of Papua New Guinea.

Mordensky, S. P., Villeneuve, M. C., Kennedy, B. M., Heap, M. J., Gravley, D. M., Farquharson, J. I., & Reuschlé, T. (2018). Physical and mechanical property relationships of a shallow intrusion and volcanic host rock, Pinnacle Ridge, Mt. Ruapehu, New Zealand. Journal of Volcanology and Geothermal Research, 359, 1-20.

Mordensky, S. P., Heap, M. J., Kennedy, B. M., Gilg, H. A., Villeneuve, M. C., Farquharson, J. I., & Gravley, D. M. (2019). Influence of alteration on the mechanical behaviour and failure mode of andesite: implications for shallow seismicity and volcano monitoring. Bulletin of Volcanology, 81, 1-12.

Mordensky, S. P., Villeneuve, M. C., Kennedy, B. M., & Struthers, J. D. (2022). Hydrothermally induced edifice destabilisation: The mechanical behaviour of rock mass surrounding a shallow intrusion in andesitic lavas, Pinnacle Ridge, Ruapehu, New Zealand. Engineering Geology, 305, 106696.

Moretti, R., Komorowski, J. C., Ucciani, G., Moune, S., Jessop, D., de Chabalier, J. B., ... & Chaussidon, M. (2020). The 2018 unrest phase at La Soufrière of Guadeloupe (French West Indies) andesitic volcano: Scrutiny of a failed but prodromal phreatic eruption. Journal of Volcanology and Geothermal Research, 393, 106769.

Moon, V., & Jayawardane, J. (2004). Geomechanical and geochemical changes during early stages of weathering of Karamu Basalt, New Zealand. Engineering geology, 74(1-2), 57-72.

Moon, V., Bradshaw, J., & de Lange, W. (2009). Geomorphic development of White Island Volcano based on slope stability modelling. Engineering geology, 104(1-2), 16-30.

Moune, S., Moretti, R., Burtin, A., Jessop, D. E., Didier, T., Robert, V., ... & Buscetti, M. (2022). Gas monitoring of volcanic-hydrothermal plumes in a tropical environment: the case of La Soufriere de Guadeloupe unrest volcano (Lesser Antilles). Frontiers in Earth Science, 10, 17.

Nara, Y., Morimoto, K., Hiroyoshi, N., Yoneda, T., Kaneko, K., & Benson, P. M. (2012). Influence of relative humidity on fracture toughness of rock: implications for subcritical crack growth. International Journal of Solids and Structures, 49(18), 2471-2481.

Nicolas, A., Fortin, J., Regnet, J. B., Dimanov, A., & Guéguen, Y. (2016). Brittle and semi-brittle behaviours of a carbonate rock: influence of water and temperature. Geophysical Journal International, 206(1), 438-456.
Nicollin, F., Gibert, D., Beauducel, F., Boudon, G., & Komorowski, J. C. (2006). Electrical tomography of La Soufrière of Guadeloupe Volcano: Field experiments, 1D inversion and qualitative interpretation. Earth and Planetary Science Letters, 244(3-4), 709-724.
Noël, C., Baud, P., & Violay, M. (2021). Effect of water on sandstone's fracture toughness and frictional parameters: Brittle strength constraints. International Journal of Rock Mechanics and Mining Sciences, 147, 104916.
Norini, G., Bustos, E., Arnosio, M., Baez, W., Zuluaga, M. C., & Roverato, M. (2020). Unusual volcanic instability and sector collapse configuration at Chimpa volcano, central Andes. Journal of Volcanology and Geothermal Research, 393, 106807.
Opfergelt, S., Delmelle, P., Boivin, P., & Delvaux, B. (2006). The 1998 debris avalanche at Casita volcano, Nicaragua: Investigation of the role of hydrothermal smectite in promoting slope instability. Geophysical Research Letters, 33(15).
Peruzzetto, M., Komorowski, J. C., Le Friant, A., Rosas-Carbajal, M., Mangeney, A., & Legendre, Y. (2019). Modeling of partial dome collapse of La Soufrière of Guadeloupe volcano: implications for hazard assessment and monitoring. Scientific Reports, 9(1), 13105.
Pola, A., Crosta, G. B., Fusi, N., & Castellanza, R. (2014). General characterization of the mechanical behaviour of different volcanic rocks with respect to alteration. Engineering Geology, 169, 1-13.
Potyondy, D. O., & Cundall, P. A. (2004). A bonded-particle model for rock. International Journal of Rock Mechanics and Mining Sciences, 41(8), 1329-1364.
Rad, S. D., Allègre, C. J., & Louvat, P. (2007). Hidden erosion on volcanic islands. Earth and Planetary Science Letters, 262(1-2), 109-124.
Reid, M. E., Sisson, T. W., & Brien, D. L. (2001). Volcano collapse promoted by hydrothermal alteration and edifice shape, Mount Rainier, Washington. Geology, 29(9), 779-782.
Reid, M. E. (2004). Massive collapse of volcano edifices triggered by hydrothermal pressurization. Geology, 32(5), 373-376.
Reid, M. E., Keith, T. E., Kayen, R. E., Iverson, N. R., Iverson, R. M., & Brien, D. L. (2010). Volcano collapse promoted by progressive strength reduction: new data from Mount St. Helens. Bulletin of volcanology, 72, 761-766.
Risnes, R., Madland, M. V., Hole, M., & Kwabiah, N. K. (2005). Water weakening of chalk—Mechanical effects of water–glycol mixtures. Journal of Petroleum Science and Engineering, 48(1-2), 21-36.
Rodell, M., Velicogna, I., & Famiglietti, J. S. (2009). Satellite-based estimates of groundwater depletion in India. Nature, 460(7258), 999-1002.
Rodríguez, A., & van Bergen, M. J. (2017). Superficial alteration mineralogy in active volcanic systems: An example of Poás volcano, Costa Rica. Journal of Volcanology and Geothermal Research, 346, 54-80.
Romero, J. E., Polacci, M., Watt, S., Kitamura, S., Tormey, D., Sielfeld, G., ... & Polanco, E. (2021). Volcanic lateral collapse processes in mafic arc edifices: a review of their driving processes, types and consequences. Frontiers in Earth Science, 9, 639825.
Rosas-Carbajal, M., Komorowski, J. C., Nicollin, F., & Gibert, D. (2016). Volcano electrical tomography unveils edifice collapse hazard linked to hydrothermal system structure and dynamics. Scientific reports, 6(1), 29899.
Rosas-Carbajal, M., Jourde, K., Marteau, J., Deroussi, S., Komorowski, J. C., & Gibert, D. (2017). Three-dimensional density structure of La Soufrière de Guadeloupe lava dome from simultaneous muon radiographies and gravity data. Geophysical Research Letters, 44(13), 6743-6751.
Rouwet, D., Tassi, F., Mora-Amador, R., Sandri, L., & Chiarini, V. (2014). Past, present and future of volcanic lake monitoring. Journal of volcanology and geothermal research, 272, 78-97.
Rutter, E. H., & Mainprice, D. H. (1978). The effect of water on stress relaxation of faulted and unfaulted sandstone. Rock Friction and Earthquake Prediction, 634-654.
Sahoo, S., Tiwari, D. K., Panda, D., & Kundu, B. (2022). Eruption cycles of Mount Etna triggered by seasonal climatic rainfall. Journal of Geodynamics, 149, 101896.
Salaün, A., Villemant, B., Gérard, M., Komorowski, J. C., & Michel, A. (2011). Hydrothermal alteration in andesitic volcanoes: trace element redistribution in active and ancient hydrothermal systems of Guadeloupe (Lesser Antilles). Journal of Geochemical Exploration, 111(3), 59-83.
Sammis, C. G., & Ashby, M. F. (1986). The failure of brittle porous solids under compressive stress states. Acta metallurgica, 34(3), 511-526.
Saucedo, R., Macías, J. L., Sarocchi, D., Bursik, M., & Rupp, B. (2008). The rain-triggered Atenquique volcaniclastic debris flow of October 16, 1955 at Nevado de Colima Volcano, Mexico. Journal of Volcanology and Geothermal Research, 173(1-2), 69-83.

Schaefer, L. N., Oommen, T., Corazzato, C., Tibaldi, A., Escobar-Wolf, R., & Rose, W. I. (2013). An integrated field-numerical approach to assess slope stability hazards at volcanoes: the example of Pacaya, Guatemala. Bulletin of Volcanology, 75, 1-18.

Schaefer, L. N., Kereszturi, G., Kennedy, B. M., & Villeneuve, M. (2023). Characterizing lithological, weathering, and hydrothermal alteration influences on volcanic rock properties via spectroscopy and laboratory testing: a case study of Mount Ruapehu volcano, New Zealand. Bulletin of Volcanology, 85(8), 43.

Scher, S., Williams-Jones, A. E., & Williams-Jones, G. (2013). Fumarolic activity, acid-sulfate alteration, and high sulfidation epithermal precious metal mineralization in the crater of Kawah Ijen Volcano, Java, Indonesia. Economic Geology, 108(5), 1099-1118.

Schmitt, L., Forsans, T., & Santarelli, F. J. (1994). Shale testing and capillary phenomena. International Journal of Rock Mechanics and Mining Sciences & Geomechanics Abstracts, 31, No. 5, 411-427.

Sens-Schönfelder, C., & Wegler, U. (2006). Passive image interferometry and seasonal variations of seismic velocities at Merapi Volcano, Indonesia. Geophysical Research Letters, 33(21).

Siebert, L., Glicken, H., & Ui, T. (1987). Volcanic hazards from Bezymianny-and Bandai-type eruptions. Bulletin of Volcanology, 49, 435-459.

Simmons, J., Elsworth, D., & Voight, B. (2004). Instability of exogenous lava lobes during intense rainfall. Bulletin of volcanology, 66, 725-734.

Singh, T. N., Singh, S. K., Mishra, A., Singh, P. K., & Singh, V. K. (1999). Effect of acidic water on physico-mechanical behaviour of rock. Indian Journal of Engineering and Materials Sciences, 6, 66-72.

Tamburello, G., Moune, S., Allard, P., Venugopal, S., Robert, V., Rosas-Carbajal, M., ... & Moretti, R. (2019). Spatio-temporal relationships between fumarolic activity, hydrothermal fluid circulation and geophysical signals at an arc volcano in degassing unrest: La Soufrière of Guadeloupe (French West Indies). Geosciences, 9(11), 480.

Tang, S. B., Yu, C. Y., Heap, M. J., Chen, P. Z., & Ren, Y. G. (2018). The influence of water saturation on the short-and long-term mechanical behavior of red sandstone. Rock Mechanics and Rock Engineering, 51, 2669-2687.

Tanguy, J-C. (1994). The 1902-1905 eruptions of Montagne Pelée, Martinique: anatomy and retrospection. Journal of Volcanology and Geothermal Research, 60: 87-107.

Taron, J., Elsworth, D., Thompson, G., & Voight, B. (2007). Mechanisms for rainfall-concurrent lava dome collapses at Soufrière Hills Volcano, 2000–2002. Journal of volcanology and geothermal research, 160(1-2), 195-209.

Tost, M., & Cronin, S. J. (2016). Climate influence on volcano edifice stability and fluvial landscape evolution surrounding Mount Ruapehu, New Zealand. Geomorphology, 262, 77-90.

Urlaub, M., Petersen, F., Gross, F., Bonforte, A., Puglisi, G., Guglielmino, F., ... & Kopp, H. (2018). Gravitational collapse of Mount Etna's southeastern flank. Science Advances, 4(10), eaat9700.

van Hinsberg, V., Berlo, K., van Bergen, M., & Williams-Jones, A. (2010). Extreme alteration by hyperacidic brines at Kawah Ijen volcano, East Java, Indonesia: I. Textural and mineralogical imprint. Journal of Volcanology and geothermal Research, 198(1-2), 253-263.

van Wyk de Vries, B., & Francis, P. W. (1997). Catastrophic collapse at stratovolcanoes induced by gradual volcano spreading. Nature, 387(6631), 387-390.

van Wyk de Vries, B., Kerle, N., & Petley, D. (2000). Sector collapse forming at Casita volcano, Nicaragua. Geology, 28(2), 167-170.

Vazquez, R., Macias, J. L., Alcala-Reygosa, J., Arce, J. L., Jimenez-Haro, A., Fernandez, S., ... & Sanchez-Nunez, J. M. (2022). Numerical modeling and hazard implications of landslides at the Ardillas Volcanic Dome (Tacana Volcanic Complex, Mexico-Guatemala). Natural Hazards, 113(2), 1305-1333.

Villemant, B., Hammouya, G., Michel, A., Semet, M. P., Komorowski, J. C., Boudon, G., & Cheminée, J. L. (2005). The memory of volcanic waters: shallow magma degassing revealed by halogen monitoring in thermal springs of La Soufrière volcano (Guadeloupe, Lesser Antilles). Earth and Planetary Science Letters, 237(3-4), 710-728.

Villemant B., Komorowski, J.-C., Dessert C., Michel A., Crispi O., Hammouya G., Beauducel F., De Chabalier, (2014). Evidence for a new shallow magma intrusion at La Soufrière of Guadeloupe (Lesser Antilles). Insights from long-term geochemical monitoring of halogen-rich hydrothermal fluids. Journal of Volcanology and Geothermal Research, 285, 247-277.

Violette, S., De Marsily, G., Carbonnel, J. P., Goblet, P., Ledoux, E., Tijani, S. M., & Vouille, G. (2001). Can rainfall trigger volcanic eruptions? A mechanical stress model of an active volcano:'Piton de la Fournaise', Reunion Island. Terra Nova, 13(1), 18-24.

Voight, B., Glicken, H., Janda, R. J. & Douglass, P. M. (1981). Catastrophic rockslide avalanche of May 18. In: Lipman, P. W. & Mullineaux, D. R. (eds) The 1980 Eruptions of Mount St Helens, Washington, US Geological Survey, Professional Papers, 1250, 347-378.

Voight, B., Komorowski J--C., Norton, G.E., Belousov, A.B., Belousova, M., Boudon, G., Francis, P.W., Franz, W., Heinrich, P., Sparks, R.S.J. & Young, S.R. (2002) The 1997 Boxing Day Sector Collapse and Debris Avalanche, Soufriere Hills Volcano, Montserrat, W.I. In: T.H. Druitt, B.P. Kokelaar (Eds), The eruption of Soufrière Hills Volcano, Montserrat, from 1995 to 1999, Geological Society, London Memoirs, 21, 363-407.

Wallace, C. S., Schaefer, L. N., & Villeneuve, M. C. (2022). Material properties and triggering mechanisms of an andesitic lava dome collapse at Shiveluch Volcano, Kamchatka, Russia, revealed using the finite element method. Rock Mechanics and Rock Engineering, 55(5), 2711-2728.

Walter, T. R., Zorn, E. U., Harnett, C. E., Shevchenko, A. V., Belousov, A., Belousova, M., & Vassileva, M. S. (2022). Influence of conduit and topography complexity on spine extrusion at Shiveluch volcano, Kamchatka. Communications Earth & Environment, 3(1), 169.

Wang, J. J., Zhu, J. G., Chiu, C. F., & Zhang, H. (2007). Experimental study on fracture toughness and tensile strength of a clay. Engineering Geology, 94(1-2), 65-75.

Wasantha, P. L., & Ranjith, P. G. (2014). Water-weakening behavior of Hawkesbury sandstone in brittle regime. Engineering Geology, 178, 91-101.

Watters, R. J., Zimbelman, D. R., Bowman, S. D., & Crowley, J. K. (2000). Rock mass strength assessment and significance to edifice stability, Mount Rainier and Mount Hood, Cascade Range volcanoes. Pure and Applied Geophysics, 157, 957-976.

Wyering, L. D., Villeneuve, M. C., Wallis, I. C., Siratovich, P. A., Kennedy, B. M., Gravley, D. M., & Cant, J. L. (2014). Mechanical and physical properties of hydrothermally altered rocks, Taupo Volcanic Zone, New Zealand. Journal of Volcanology and Geothermal Research, 288, 76-93.

Yamasato, H., Kitagawa, S., Komiya, M. (1998). Effect of rainfall on dacitic lava dome collapse at Unzen volcano, Japan. Papers in Meteorology and Geophysics, 48(3), 73-78.

Yilmaz, T. I., Wadsworth, F. B., Gilg, H. A., Hess, K. U., Kendrick, J. E., Wallace, P. A., ... & Dingwell, D. B. (2021). Rapid alteration of fractured volcanic conduits beneath Mt Unzen. Bulletin of Volcanology, 83, 1-14.

Young, S., Voight, B., Barclay, J., Herd, R.A., Komorowski, J-C., Miller, A.D., Sparks, R.S.J., Stewart, R.C. (2002). Hazard implications of small-scale edifice instability and sector collapse: a case history from Soufriere Hills volcano, Montserrat. In: T.H. Druitt, B.P. Kokelaar (eds), The eruption of Soufrière Hills Volcano, Montserrat, from 1995 to 1999, Geological Society, London, Memoirs, 21, 349-361

Zimbelman, D. R. (1996). Hydrothermal alteration and its influence on volcanic hazards--Mount Rainier, Washington, a case history. University of Colorado at Boulder.

Zimbelman, D. R., Rye, R. O., & Breit, G. N. (2005). Origin of secondary sulfate minerals on active andesitic stratovolcanoes. Chemical Geology, 215(1-4), 37-60.

Zhu, W., Baud, P., & Wong, T. F. (2010). Micromechanics of cataclastic pore collapse in limestone. Journal of Geophysical Research: Solid Earth, 115(B4).

Zhu, W., Baud, P., Vinciguerra, S., & Wong, T. F. (2011). Micromechanics of brittle faulting and cataclastic flow in Alban Hills tuff. Journal of Geophysical Research: Solid Earth, 116(B6).

Zhu, W., Baud, P., Vinciguerra, S., & Wong, T. F. (2016). Micromechanics of brittle faulting and cataclastic flow in Mount Etna basalt. Journal of Geophysical Research: Solid Earth, 121(6), 4268-4289.